



2014

# NUMERICAL ANALYSIS OF DROPLET FORMATION AND TRANSPORT OF A HIGHLY VISCOUS LIQUID

Peiding Wang

*University of Kentucky*, wangpeiding@gmail.com

---

## Recommended Citation

Wang, Peiding, "NUMERICAL ANALYSIS OF DROPLET FORMATION AND TRANSPORT OF A HIGHLY VISCOUS LIQUID" (2014). *Theses and Dissertations--Mechanical Engineering*. Paper 44.  
[http://uknowledge.uky.edu/me\\_etds/44](http://uknowledge.uky.edu/me_etds/44)

This Master's Thesis is brought to you for free and open access by the Mechanical Engineering at UKnowledge. It has been accepted for inclusion in Theses and Dissertations--Mechanical Engineering by an authorized administrator of UKnowledge. For more information, please contact [UKnowledge@lsv.uky.edu](mailto:UKnowledge@lsv.uky.edu).

**STUDENT AGREEMENT:**

I represent that my thesis or dissertation and abstract are my original work. Proper attribution has been given to all outside sources. I understand that I am solely responsible for obtaining any needed copyright permissions. I have obtained and attached hereto needed written permission statement(s) from the owner(s) of each third-party copyrighted matter to be included in my work, allowing electronic distribution (if such use is not permitted by the fair use doctrine).

I hereby grant to The University of Kentucky and its agents the irrevocable, non-exclusive, and royalty-free license to archive and make accessible my work in whole or in part in all forms of media, now or hereafter known. I agree that the document mentioned above may be made available immediately for worldwide access unless a preapproved embargo applies. I retain all other ownership rights to the copyright of my work. I also retain the right to use in future works (such as articles or books) all or part of my work. I understand that I am free to register the copyright to my work.

**REVIEW, APPROVAL AND ACCEPTANCE**

The document mentioned above has been reviewed and accepted by the student's advisor, on behalf of the advisory committee, and by the Director of Graduate Studies (DGS), on behalf of the program; we verify that this is the final, approved version of the student's dissertation including all changes required by the advisory committee. The undersigned agree to abide by the statements above.

Peiding Wang, Student

Dr. Kozo Saito, Major Professor

Dr. James McDonough, Director of Graduate Studies

---

NUMERICAL ANALYSIS OF DROPLET FORMATION  
AND TRANSPORT OF A HIGHLY VISCOUS LIQUID

---

THESIS

---

A thesis submitted in partial fulfillment of the  
requirements for the degree of Master of Science  
in Mechanical Engineering in the College of  
Engineering at the University of Kentucky

By

Peiding Wang

Lexington, Kentucky

Co-Directors: Dr. Kozo Saito, Professor of  
and Dr. Nelson Akafuah, Assistant Research Professor of

Mechanical Engineering

Lexington, Kentucky

2014

Copyright© Peiding Wang 2014

## ABSTRACT OF THESIS

### NUMERICAL ANALYSIS OF DROPLET FORMATION AND TRANSPORT OF A HIGHLY VISCOUS LIQUID

Drop-on-demand (DOD) inkjet print-head has a major share of the market due to simplicity and feasibility of miniature system. The efficiency of droplet generation from DOD print-head is a result of several factors, include viscosity, surface tension, nozzle size, density, driving waveform (wave shape, frequency, and amplitude), etc. Key roles in the formation and behavior of liquid jets and drops combine three dimensionless groups: Reynolds number, Weber number and Ohnesorge number. These dimensionless groups provide some bounds to the “printability” of the liquid. Adequate understanding of these parameters is essential to improve the quality of droplets and provide guidelines for the process optimization. This thesis research describes the application of computational fluid dynamics (CFD) to simulate the creation and evolution process of droplet generation and transport of a highly viscous Newtonian fluid. The flow field is governed by unsteady Navier-Stokes equations. Volume of Fluid (VOF) model is used to solve this multi-phase (liquid-gas) problem.

KEYWORDS: drop-on-demand, droplet generation, satellite droplets, numerical simulation, high viscosity

---

Peiding Wang

---

08/07/2014

---

NUMERICAL ANALYSIS OF DROPLET FORMATION  
AND TRANSPORT OF A HIGHLY VISCOUS LIQUID

By  
Peiding Wang

Dr. Kozo Saito

---

Director of Thesis

Dr. Nelson Akafuah

---

Co-Director of Thesis

Dr. James M. McDonough

---

Director of Graduate Studies

08/07/2014

---

## ACKNOWLEDGMENTS

Foremost, I would like to express my deepest gratitude to my advisor Professor Kozo Saito for his continuous support and excellent guidance during my master's studies. His insightful and ingenious comments helped me in all the time of research and writing this thesis. I am also grateful to my co-advisor Professor Nelson Akafuah for his guidance, encouragement and countless suggestions throughout my studies and research. I am thankful for the useful discussions by both Dr. Tianxiang Li and Dr. Ahmad A. Salameh. And I would also like to thank my advisory committee member Professor Tim Wu for providing exceptional suggestions and invaluable discussions.

Besides, I would like to thank my lab mates in IR4TD: Sadegh Poozesh, Li Yang, Justin English, Brittany Adam, Jeremiah Fugate, Yunqing Han, Anthony Adornato. We discuss and share our research work together every week, and have fun during the last two years.

Finally, I thank my parents who always support and love me.

## TABLE OF CONTENTS

ACKNOWLEDGMENTS.....	iii
LIST OF TABLES.....	vi
LIST OF FIGURES.....	vii
Chapter 1: Introduction	
Background and Motivation.....	1
Droplet Generation Process.....	2
Material Properties that Influence Droplet Generation.....	4
Research Objectives.....	5
Chapter 2: Literature Review	
Droplet Formation in DOD Inkjet.....	7
Droplet Size and Speed.....	8
Forces Involved in Droplet Formation.....	10
Satellite Droplet Formation.....	12
Overview of Inkjet Technology.....	13
Review CFD Application to Droplet Formation.....	17
Chapter 3: Numerical Modeling Approach	
Basic Assumptions.....	19
Model and Computational Geometry.....	21
Governing Equations.....	22
Basic Conservation Equations.....	22
Initial and Boundary Conditions.....	23
Multi-Phase Flow Equations and Volume of Fluid (VOF) Model.....	24
Chapter 4: CFD Simulation Results Analysis	
Influence of Nozzle Size on DOD Droplet Generation.....	28
Influence of Actuation Frequency.....	33

Influence of Actuation Wave Peak-to-Valley Ratio.....	39
Influence of Actuation Wave Shape.....	43
Influence of Nozzle Inner Wall Contact Angle.....	46
Droplets Transport.....	49
Chapter 5 Conclusion and Recommendation	
Summaries and Conclusions.....	52
Recommendations.....	54
Appendix	
Liquid Inlet User Defined Function (UDF) Code.....	56
References.....	58
Vita.....	61



LIST OF TABLES

Table 4.1, Droplet velocity record for different actuation frequency: 40 kHz,  
50 kHz, 60kHz, 70 kHz, and 80 kHz.....37

## LIST OF FIGURES

Figure 1.1, 6 Stages of droplet formation process.....	3
Figure 2.1, Classification of inkjet technology.....	14
Figure 2.2, Principle of CIJ system.....	14
Figure 2.3, The first drop-on-demand inkjet device.....	15
Figure 2.4, Classification of Piezo inkjet print-head by deformation mode.....	17
Figure 3.1, Print-head model.....	21
Figure 3.2, Computational geometry and grid.....	22
Figure 4.1, Droplet generation of high viscous liquid with viscosity $0.1003 \text{ kg / m - s}$ . From up to bottom on each figure: nozzle size = $30 \mu\text{m}$ , $40\mu\text{m}$ , $50\mu\text{m}$ .....	30
Figure 4.2, Break-up Length with different nozzle diameter for a series of initial ejection velocity.....	32
Figure 4.3, Break-up time with different nozzle diameter for a series of initial ejection velocity.....	33
Figure 4.4, Droplet formation of high viscous liquid. Nozzle diameter is $30 \mu\text{m}$ . In each image, from up to bottom: actuation frequency = $40 \text{ kHz}$ , $50 \text{ kHz}$ , $60 \text{ kHz}$ , $70 \text{ kHz}$ , and $80 \text{ kHz}$ . Images are presented every $20 \mu\text{s}$ from $40 \mu\text{s}$ to $100 \mu\text{s}$ .....	34
Figure 4.5, Droplet formation of high viscous liquid. Nozzle diameter is $40 \mu\text{m}$ . In each image, from up to bottom: actuation frequency = $40 \text{ kHz}$ , $50 \text{ kHz}$ , $60 \text{ kHz}$ , $70 \text{ kHz}$ , and $80 \text{ kHz}$ . Images are presented every $20 \mu\text{s}$ from $40 \mu\text{s}$ to $100 \mu\text{s}$ .....	35
Figure 4.6, Droplet formation of high viscous liquid. Nozzle diameter is $50 \mu\text{m}$ . In each image, from up to bottom: actuation frequency = $40 \text{ kHz}$ , $50 \text{ kHz}$ , $60 \text{ kHz}$ , $70 \text{ kHz}$ , and $80 \text{ kHz}$ . Images are presented every $20 \mu\text{s}$ from $40 \mu\text{s}$ to $100 \mu\text{s}$ .....	36
Figure 4.7, Droplet velocity record for different actuation frequency: $40 \text{ kHz}$ , $50 \text{ kHz}$ , $60\text{kHz}$ , $70 \text{ kHz}$ , and $80 \text{ kHz}$ .....	38
Figure 4.8, Four selected peak-to-valley ratio wave form.....	39
Figure 4.9, Three DOD droplet generation with a peak-to-valley ratio 1:1.	

From top to bottom, images begin from 00 $\mu$ s to 100 $\mu$ s. Time interval is 10 $\mu$ s.....	40
Figure 4.10, Three DOD droplet generation with a peak-to-valley ratio 1:2.	
From top to bottom, images begin from 00 $\mu$ s to 100 $\mu$ s. Time interval is 10 $\mu$ s.....	41
Figure 4.11, Three DOD droplet generation with a peak-to-valley ratio 1:3.	
From top to bottom, images begin from 00 $\mu$ s to 100 $\mu$ s. Time interval is 10 $\mu$ s.....	41
Figure 4.12, Three DOD droplet generation with a peak-to-valley ratio 1:4.	
From top to bottom, images begin from 00 $\mu$ s to 100 $\mu$ s. Time interval is 10 $\mu$ s.....	42
Figure 4.13, Images of DOD droplet generation of different peak-to-valley ratio. Images are recorded at 80 $\mu$ s. From top to bottom on each image, peak-to-valley ratio = 1:1, 1:2, 1:3, and 1:4. Actuation frequency = 60kHz.....	43
Figure 4.14, Sinusoidal and square wave form. X axis is the elapsed time, Y axis is the velocity of liquid column before the formation of droplet.....	44
Figure 4.15, Simulation results of droplet generation of (a) sinusoidal wave and (b) square wave. Each of image (a) and (b), from top to bottom, begins when liquid emerges from the nozzle and shown for every 10 $\mu$ s throught 100 $\mu$ s.....	45
Figure 4.16, Droplet generation with the nozzle wall contact angle of 0°.	
From top to bottom, the time for each image is: 8.4 $\mu$ s, 17.7 $\mu$ s, 37.3 $\mu$ s, 75.6 $\mu$ s, 138.0 $\mu$ s, 181.0 $\mu$ s, 280 $\mu$ s, 300 $\mu$ s.....	46
Figure 4.17, Droplet generation with the nozzle wall contact angle of 45°.	
From top to bottom, the time for each image is: 8.4 $\mu$ s, 17.7 $\mu$ s, 37.3 $\mu$ s, 75.6 $\mu$ s, 138.0 $\mu$ s, 181.0 $\mu$ s, 280 $\mu$ s, 300 $\mu$ s.....	47
Figure 4.18, Droplet generation with the nozzle wall contact angle of 90°.	

From top to bottom, the time for each image is: 8.4 $\mu$ s, 17.7 $\mu$ s, 37.3 $\mu$ s, 75.6 $\mu$ s, 138.0 $\mu$ s, 181.0 $\mu$ s, 280 $\mu$ s, 300 $\mu$ s.....	47
Figure 4.19, Droplet generation with the nozzle wall contact angle of 135°.	
From top to bottom, the time for each image is: 8.4 $\mu$ s, 17.7 $\mu$ s, 37.3 $\mu$ s, 75.6 $\mu$ s, 138.0 $\mu$ s, 181.0 $\mu$ s, 280 $\mu$ s, 300 $\mu$ s.....	48
Figure 4.20, Droplet generation with the nozzle wall contact angle of 180°.	
From top to bottom, the time for each image is: 8.4 $\mu$ s, 17.7 $\mu$ s, 37.3 $\mu$ s, 75.6 $\mu$ s, 138.0 $\mu$ s, 181.0 $\mu$ s, 280 $\mu$ s, 300 $\mu$ s.....	48
Figure 4.21, The velocity variation of the first droplet with different contact angle.....	49
Figure 4.22, Droplet travels long distance without air flow. These 3 images are recorded at time: 30 $\mu$ s, 40 $\mu$ s and 85 $\mu$ s.....	50
Figure 4.23, A series droplets generation with a right-direction air flow of 5m/s. These 3 images are recorded at time: 30 $\mu$ s, 40 $\mu$ s and 85 $\mu$ s.....	50
Figure 4.24, A series droplets generation with a right-direction air flow of 15 m/s. These 4 images are recorded at time: 30 $\mu$ s, 40 $\mu$ s, 77 $\mu$ s and 85 $\mu$ s.....	51

## Chapter 1 Introduction

### 1.1 Background and Motivation

The basic principle of transformation from bulk fluid to droplets has remained the same for hundreds of years. This transformation process is of great importance in several industrial applications, such as automotive painting, inkjet printing, medicine and agriculture. During the past decades, there has been a tremendous effort devoted to the droplets generation work on basic theory and device improvement. With different patterns of machines, bulk fluid can be produced to two types of droplets. First is called spray, which produces large amount of droplets with a wide range of droplet size. The second pattern, which we will concentrate on in this study, has a narrower droplet size distribution.

In inkjet printing industry, to achieve reliable operation, unique and small droplet size is desired. Inkjet printing technology produces small size droplets, typically 10 – 100  $\mu\text{m}$  in diameter. Investigations reveals that many methods have been developed for inkjet droplet generation. Most of them falls into two main categories described as continuous inkjet (CIJ) and drop-on-demand inkjet (DOD) [1]. In continuous inkjet, as the name implies, the flow is continuous, while in Drop-on-demand inkjet, the flow is impulsive. In CIJ technology, a high-pressure pump directs liquid ink from a reservoir through a gunbody and a microscopic nozzle, creating a continuous stream of ink droplets by Plateau-Rayleigh instability [2]. This series of droplets charged by a charging electrode fly though an electrostatic field. Deflection plates direct droplets to collection gutter for

re-use or to hit on substrate. CIJ allows the fluid flow with relatively high speed (~50m/s), thus enable long distance transport and high-frequency ejection. In DOD technology, two strategies are employed for actuation. These two mechanisms are thermal actuation and piezoelectric actuation. When applying a voltage pulse, the deformation of piezoelectric actuator or vaporization of thermal actuator cause a large pressure increase, propelling a column of ink ejected out of nozzle. DOD is operated with lower cost because it works without deflection devices. DOD shares large part of inkjet market due to this simplicity. Surface tension, inertia and viscosity play key roles in the generation and behavior of liquid droplets. Three essential dimensionless numbers can be used to characterize the importance and influence of the above parameters: Reynolds number, Weber number and Ohnesorge number.

In order to predict the behavior of droplet generation of high viscous liquid in micron scale, a fully understanding of the generation process is of great importance.

Investigations reveal that previous research focus on droplet with viscosity mostly below 20 cP (about 20 times of viscosity of water) in macro scale. However, high viscous paints are widely used in painting industry, and there is no comprehensive description of disintegration and transportation process of high viscous liquid. Micro scale inkjet printing process is different from macro scale spray due to capillary, surface tension and instability.

## 1.2 Droplet Generation Process

In order to predict the behavior of droplets, a comprehensive understanding of the droplet generation process is essential.

Droplet formation is a dynamic process. Figure 1.1 describe 6 different stages of single droplet formation process [1, 3].

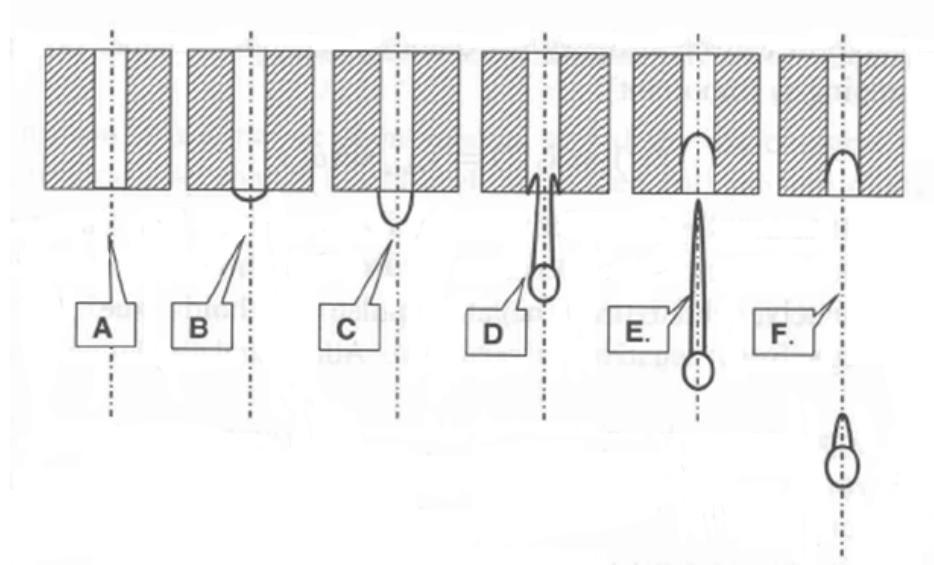


Figure 1.1 6 Stages of droplets formation process

Before the application of charges to the actuator, liquid inside nozzle stays at equilibrium state. Liquid velocity and pressure are zero at that stage. When the actuator is applied stimulation, high pressure is generated inside nozzle and the liquid start to flow out of the orifice. In the meantime, kinetic energy is transported from actuator walls to outflow. Kinetic energy is undergoing an attenuation process, because it overcomes the resistance from surface tension. Afterwards, the droplet is connected with the liquid inside the nozzle by a skinny fluid filament. After some time, if the liquid column momentum is large enough, the droplet will escape from the nozzle. Surface tension is the acting force to pinch off the ligament. The meniscus retracts inside the

nozzle. And when reservoir finish refilling the nozzle, the process recycle again from equilibrium stage.

### 1.3 Material Properties that Influence Droplet Generation

The droplet generation process is determined by several parameters. They take effect from applying actuation to the pinch-off of ligament. The influential parameters of droplet generation falls into three categories: fluid properties, nozzle geometry and driving waveform.

Three physical properties of liquid play important role during this whole process:

viscosity, surface tension and fluid density. Surface tension is a contractive tendency of the surface of a liquid that allows it to resist an external force. Liquid atoms or molecules at a free surface have higher energy than those inside the liquid body. Thus the shape of liquid with lowest surface tension energy is sphere. The character that a liquid tend to form a shape with lowest energy is essential to the droplet generation.

During droplet generation process, the attraction of water to each other is greater than the molecules in the air. The net effect is an inward force at its surface to cause water to behave as if its surface were covered by a stretched elastic membrane. This is also the major cause of pinch-off effect [4]. Most liquids used in inkjet printing have surface tension of the order of tens of dyn/cm (or mN/m). For example, pure water at 20°C, surface tension equals 72.5 dyn/cm. Viscosity and inertia generate forces that resist the deformation of liquid jet. Viscous force arise from the interaction of molecules of the liquid and act between regions of liquid moving relative to each other [5]. Pure water



has a viscosity of 1 cP (mPas). And other liquids used in inkjet printing usually have viscosity ranging from 2 to 100 cP [6]. Inertial force is associated with the change of momentum in a liquid which is proportional to the liquid density and the rate of change of velocity.

Nozzle size is a significant geometry property that influence droplet generation. Printing quality is limited by the size of the droplet, which ultimately influenced by the diameter of print-head nozzle. The nozzle size should theoretically form the lower bound of the droplet size.

When a signal is applied to the actuator of a print-head, the actuator responds, producing a pressure inside the chamber. As a result, the liquid is ejected outward. The droplet generation dynamics is mostly affected by the waveform of the actuation signal. The waveform includes wave shape, wave frequency, and amplitude of wave.

#### 1.4 Research Objectives

The primary study objectives of this thesis are summarized as follows:

- To introduce the general process of and the factors that influence droplet generation. Several dimensionless groups combined by these factors are studied. A series of CFD simulations will be conducted to study these factors.
- To present literature review of related topics, such as droplet formation, forces involved in droplet formation and transportation, inkjet technology, CFD application in droplet formation, as a form of background and overview of existing research.

- To study the formulations of two phase flow problem in this VOF (Volume-of-Fluid) model employed by CFD simulation.
- To use existing experimental and simulation results obtained by other authors to corroborate the CFD results in this article.

In the subsequent chapters, these objectives will be further expanded.

## Chapter 2 Literature Review

### 2.1 Droplet Formation in DOD Inkjet

In this section, we reviewed several previous research on droplet formation process in Drop-On-Demand inkjet printing. After the first DOD device was invented in 1940s, tremendous research work has been devoted into the mechanism of droplet formation especially on Newtonian fluids. During recent years, as more and more Non-Newtonian fluids have been widely used in industry, Non-Newtonian fluids attract more eyes. Micro scale droplet generation differs from macro scale droplet generation owing to not only the tens of micron length but also the time scale is less than a hundred micro-second. This is the major reason to make the whole process difficult to observe.

Shin *et al.* [7] and Verkouteren *et al.* [8] were able to observe and record the transient process of droplet generation using a charge coupled device (CCD). Dong and Carr [9] [10] studied the dynamics of drop-on-demand (DOD) droplet formation using an imaging system with an inter-frame time of 1  $\mu$ s. Their experiment were conducted on a range of viscosities (1.0 - 5.0 cP) and surface tensions (35 – 73 mN/m). They observed that main stages of droplet formation include ejection and stretching of liquid, pinch-off of liquid thread from the nozzle exit, contraction of liquid thread, break-up of liquid thread into primary droplet and satellites, and recombination of primary droplet and satellites. After analyzing their experimental results, they proposed an essential requirement for the recombination of primary droplet and satellite droplets and the limit for liquid thread length without break-up during contraction. Evans *et al.* [11]

discussed major factors in controlling the quality of the resultant printed image is the way in which the ink droplet is formed and the consistency of this process. They used traditional ink as the starting point and used a range of polymers with different molecular weights and viscosity as an additive. Lopez *et al.* [12] studied the combination effect of ink rheological behavior and the waveform signal applied to produce the droplet. Their research focus on the dynamics of filament break-up and the transient contraction of the filament being swallowed in the droplet following break-off. Desheng *et al.* [13] studied the influence of polymer concentration on DOD inkjet printing for concentrations from dilute through the overlap regimes and the ligament formation during DOD inkjet printing of solutions. They found the physical behavior of the fluids in droplet formation is due to the dominance of viscoelastic effects within the timescale of the process, in preventing ligament break-up at the pinch point compared with a Newtonian fluid of similar viscosity. The distance travelled by the primary droplet and droplet velocity was found to depend only on the applied voltage.

## 2.2 Droplet Size and Speed

In a typical inkjet droplet generation process, droplet velocity and droplet size are directly determined by the droplet volume and initial velocity. Wijshoff [14] and Sakai [15] discussed the estimate of the droplet size with reference printhead design and the traveling wave principle based on experimental observation. They start with a cylinder as the shape of the ink column flows outwards. The nozzle area multiply the length of the liquid column equals the column volume. And the droplet velocity times droplet formation time equals the length of the liquid column. The droplet formation time is

determined by the parameters of width of the driving wave form, the nozzle shape and ink properties. In which, the width of driving wave form is for the maximum efficiency tuned to the travel time of the acoustic wave. The nozzle shape impacts on the acoustic impedance. Ink properties include viscosity and surface tension. The travel time of the acoustic wave is given by the channel length, the inlet geometry of the supply and the effective speed of sound inside the chamber. The effective speed of sound is given by the speed of sound of the ink itself and the compliance of the channel cross-section, as defined by the Eq. (1)

$$c_{eff} = c\sqrt{B_{ch}} = \sqrt{B_{ch}} \sqrt{\frac{c_0^2}{1 + \rho c_0^2 \beta}} \quad (1)$$

And  $B_{ch}$  is a function of the integral of the velocity profile over the channel cross-section,  $c$  is the speed of sound of the ink,  $\beta$  is the compliance of the channel cross-section,  $c_0$  is the local speed of sound,  $\rho$  is the liquid density.

Dijksman [16] has given another simpler approximate method to determine the droplet speed and size. He assumed the ink outside the nozzle moves with the same velocity as the ink inside the nozzle. The nozzle is considered to be completely filled all the time as with the acoustic calculations. The criterion for droplet formation is that a droplet is formed when the kinetic energy of the ink volume outside the nozzle becomes equal to the integral over time of the kinetic energy at the nozzle exit, minus the surface energy of the ink outside the nozzle. The droplet size is calculated as nozzle area times the integral over time of the average ink speed, which is based on acoustic calculations. The

droplet speed is calculated from the resulting kinetic energy with corrections for breakup and the viscous losses to form a spherical droplet.

Cittadino et al. [17] developed a non-linear model to predict the velocity of the ejected droplet. This approach, which is based on a balance of forces, shows that the ejection velocity is strong a function of the applied voltage.

Feng and James [18] proposed an even simpler approach which is based on a series of numerical calculations on Flow3D. This reference provide an insight into the droplet ejection behavior for establishing general design rules in device development. And it shows that the volume of ejected droplet is very close to the volume of fluid pushed through the nozzle by an actuation pulse. The speed of the ejected droplet is typically between one third and two thirds of the average velocity of the fluid pushed through the nozzle during actuation.

### 2.3 Forces Involved in Droplet Formation

We have discussed the properties that influence the droplet generation process in previous section. These properties determine three important forces during the process.

The three forces are viscous force, surface tension force and inertial force. Two significant dimensionless numbers can be used to characterize the relationship and relative importance among these forces: the Weber number and Reynolds number.

Weber number can be thought of as a measure of the relative importance of the fluid's inertia compared to its surface tension [19]. It is named after Moritz Weber (1871-1951) and is defined by:

$$We = \frac{\rho V^2 d}{\sigma} \quad (2)$$

Where

$\rho$  is the density of fluid,

$V$  is the velocity,

$d$  is its characteristic length, typically the droplet diameter or the nozzle diameter,

$\sigma$  is the surface tension.

The Reynolds number is defined as the ratio of inertial forces to viscous forces. Osborne Reynolds (1842-1912) popularized the use of this number in 1883, thus it is named after him [20-23], and it is generally defined by:

$$Re = \frac{\rho d V}{\eta} \quad (3)$$

Where

$\eta$  is the viscosity of the fluid.

Sometimes we need to take away the influence of the velocity. Wolfgang von Ohnesorge defined a dimensionless number named after him in his 1936 doctoral dissertation [24]. The Ohnesorge number (Oh) relates the viscous forces to inertial force and surface tension force. It is defined as:

$$Oh = \frac{\sqrt{We}}{Re} = \frac{\eta}{\sqrt{\sigma\rho d}} \quad (4)$$

The Ohnesorge number only reflects the the physical properties of the liquid and the size of the droplet. And it is independent of the driving conditions. When the Ohnesorge number is too high, usually  $Oh > 1$ , the viscous force is large enough to prevent the separation of the droplet. While when it is too low, mostly  $Oh < 0.1$ , the surface tension dominates this process and the liquid jet will break up into a large number of satellite droplets.

#### 2.4 Satellite Droplets Formation

Single droplet is desired for most inkjet printing applications. However, extra droplets are occasionally generated due to the collapse of the liquid column by surface tension. These satellite droplets are usually smaller than intended primary droplet. Satellite droplets cause several problems for printing [25]. If these unexpected droplets do not land on the place where primary droplets land, they will result in the degradation of print quality, leading to contamination or failure. This is most clearly seen in the blurring of the trailing edge of a printed area [1] [26].

Wijshoff [27] described four types of satellite droplets generation mechanisms. The first type is mist of droplets. The droplet tail travels with primary droplet, however it is unstable when it becomes smaller and smaller. A certain source of perturbation will get enough amplitude to destabilize the tail. As a result, the small tail will break up randomly or another micro-thread will be formed randomly. The second type is known



as Rayleigh instability. Generally the droplet is of high velocity. At this situation a long tail will be formed, which is unstable. At this time, capillary waves are excited by perturbation. However currently the perturbation is not the direct cause for breakup, it is only the initiation for break up. After that, the radius is reduced further due to surface tension. And finally, the long tail break up. The third type of satellite is a part of the droplet moves away in front of the head of the droplet. This kind of satellite droplets results from a supercritical acceleration at the start of the droplet formation process. Mostly, when liquid flows from the tail to the head of the droplet and surface tension is able to hold the liquid together. But if some part of liquid exceed the maximum velocity, a new spherical droplet is formed. The fourth type of satellite, slow satellite, similarly is caused by a part of liquid with slow velocity.

## 2.5 Overview of Inkjet Technology

The inkjet technology developed rapidly start from 1940s. Many methods for droplet generation have been invented since then. Currently, the most widely used two methods for inkjet printing technology are categorized in two ways: continuous inkjet (CIJ) and Drop-on-Demand inkjet (DOD) [28].

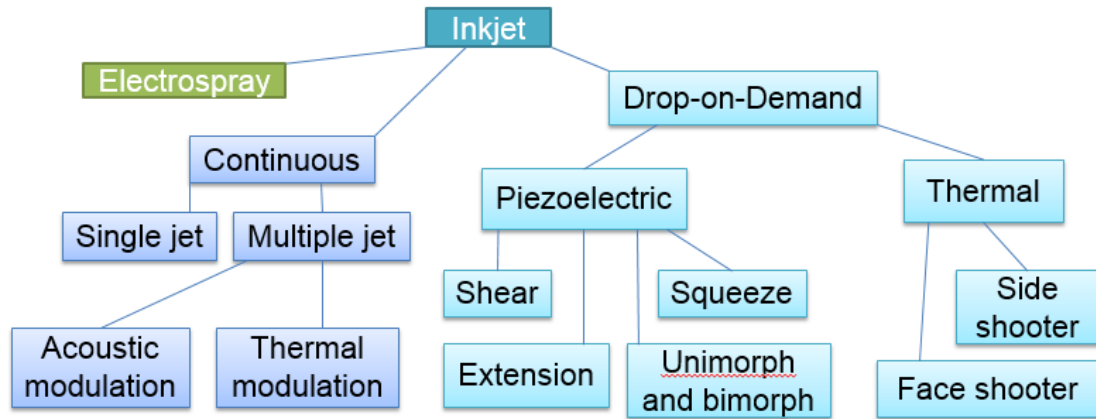


Figure 2.1: Classification of inkjet technology

Continuous ink jet, as the name indicates, the liquid flow is continuous. A high-pressure actuator directs liquid ink from a reservoir through a nozzle, creating a continuous stream of ink droplets by the mechanism of Plateau-Rayleigh instability [28].

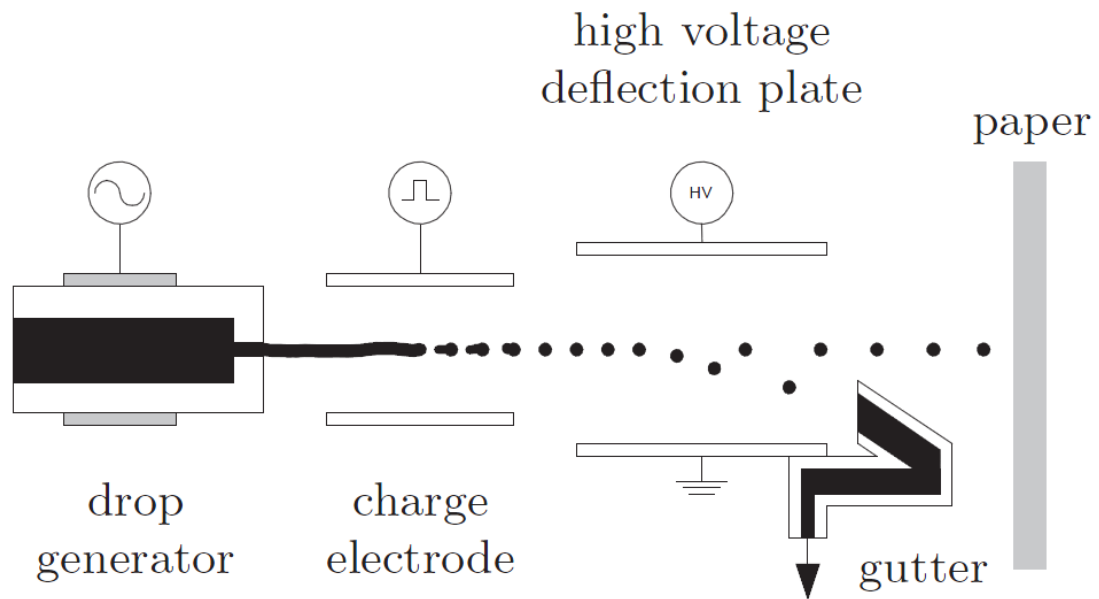


Figure 2.2: Principle of CIJ system [30]

By adding periodic (acoustic) actuation, the random droplet formation process becomes synchronized to that period as was predicted by Lord Rayleigh. Consequently, the resulting droplets can be charged and pass through an electrostatic field and are

deflected by electrostatic deflection plates to print on the desired position. Some droplets are directed to hit on a collection gutter for re-use.

Instead of continuously firing droplets, drop-on-demand inkjet create droplets only when an actuation is applied to the actuator. The primary advantages of drop-on-demand inkjet over continuous inkjet is that there is no need for complicated hardware for break-off synchronization, charging electrodes, deflection electrodes, guttering, and re-circulation systems, high-pressure ink supplies and complex electronic circuitry [27].

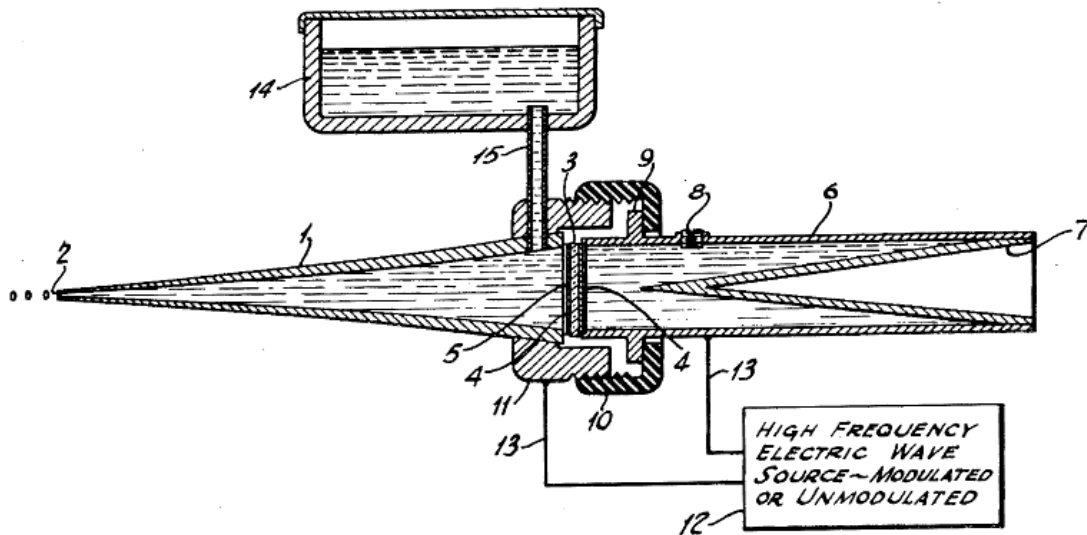


Figure 2.3: The first drop-on-demand inkjet device [31]

Most commercial and industrial inkjet printers use a piezoelectric material in an ink-filled chamber behind the nozzle. When a voltage is applied, the piezoelectric material changes shape and generates a pressure to force the liquid out.

Generally, the basis of piezo-electrical inkjet (PIJ) printers is attributed to three patents [32]. The first one is that of Zoltan of the Clevite company (US Patent 3,683,212) [33], proposing a squeeze mode of operation. The second one of Stemme of the Chalmer

University (US Patent 3,747,120) [34] utilizes the bend mode of piezoelectric operation. Finally, Kyser and Sears of the Silonics Company (US Patent 3,946,398) [35] used a diaphragm mode of operation. Common denominator of these three patents is the use of a piezoelectrical unit to convert a pulse of electrical energy into a mechanical pressure to overcome the surface tension forces holding the ink at a nozzle. Droplets are only created when an actuation pulse is provided, hence drop-on-demand. Obviously, the main discriminator between these patents is the used dominating deformation mode of the piezoelectric material together with the geometry of the ink channels. The patents of Howkins (US Patent 4,459,601) [36] describing the push mode version and Fischbeck (US Patent 4,584,590) [37] proposing the shear mode, completed the now commonly adapted categorization of printhead configurations. Generally, four types of piezoelectric printheads can be named with squeeze, push, bend, and shear mode, as shown in Fig. 2.4.

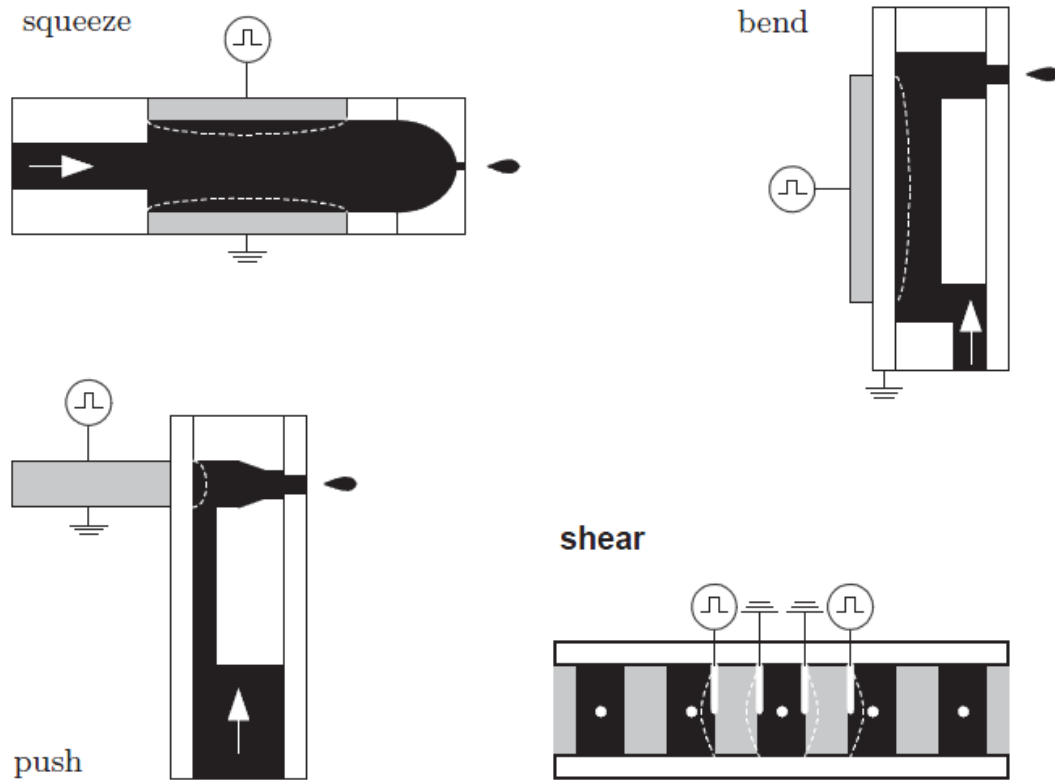


Figure 2.4: Classification of Piezo inkjet print-head by deformation mode

## 2.6 Review CFD Application to Droplet Formation

Micro scale ink jet printing process is of the tens of micron length and the time scale is less than a hundred micro-second. This character makes the process very difficult to record and observe. In addition, experimental devices are extremely expensive and complicated. Computational fluid dynamics (CFD) is a new method to simulate the droplet generation process with low cost. Volume-of-fluid (VOF) model is found to be an appropriate multiphase flow model to be performed on liquid break-up and droplet formation. Commercial software ANSYS FLUENT, Flow3D are skilled in this application.

Adams *et al.* [38] and Shield *et al.* [39] developed one-dimensional models. They obtained good qualitative results with less complex approach.

Fromm [40] discussed used a complete incompressible flow equations with a free surface and studied an impulsively driven laminar jet. His model predict the transitions from symmetric flow for a low-viscosity Newtonian fluid to asymmetric inertial viscous flow. Feng *et al.* [18] explored the general design rules in ink jet printing device development with CFD calculation. The computational results show that the volume of ejected droplet is very close to the volume of fluid pushed through the nozzle by an actuation pulse. The speed of the ejected droplet is typically between one third and two thirds of the average velocity of the fluid pushed through the nozzle during actuation. The conditions for obtaining various (desirable or undesirable) droplet shapes immediately after ejection are examined.

Xu and Basaran [41] simulated the formation of liquid droplets of incompressible Newtonian fluids from a simple capillary tube by imposing a transient flow rate upstream of the nozzle exit.

Castrejon-Pita *et al.* [42] used experimental results as initial condition in Lagrangian finite-element simulations. He compared the behavior of satellite droplets and speed of droplet motion with experimental results.

## Chapter 3 Numerical Modeling Approach

In this chapter, we describe the modeling approach, which includes basic assumptions, governing equations, boundary conditions, and numerical models employed in our simulations.

### 3.1 Basic Assumptions

To make our numerical calculations realizable and achievable, we should make several assumptions that only contains the essential control mechanisms but disregard less influential factors. For all the numerical simulations, we assume:

1. The internal and external flows are laminar.
2. The whole process from droplet generation to droplet transport can be regarded as axisymmetric.
3. The surrounding air can be considered as incompressible.
4. The liquid properties are known and constant.
5. The evaporation of the liquid is ignored.
6. The gravitational effect is neglected because it is trivial compared with other forces.

Small geometry size of the painting nozzle and droplet ( $d=30 \sim 50$  microns) and the relatively low velocity ( $9.26 \sim 18.51$  m/s) results in a relatively low Reynolds number range ( $3 \sim 10$ ). Thus the flow of the droplet generation falls in laminar regime. Therefore the laminar flow is an appropriate assumption in droplet generation.

The second assumption is based on the axisymmetric geometry. As the fluid flow is laminar flow (assumption 1), we suppose there is no swirl generated in the fluid. Therefore, the azimuthal direction flow (including eddies and fluctuations) is absent. And axisymmetric assumption holds. In addition, axisymmetric simulations are 2-D, which allows excellent accuracy while being relatively inexpensive.

Most part of the surrounding air is still. Only very small part of the air can be moved by droplets. However the velocity is relatively slow and the Mach number is definitely below 0.3. Thus we consider the surrounding air as incompressible.

The liquid we use during our numerical simulation is Newtonian fluid. Assumption 4 is a simplification for Newtonian fluids investigation.

Assumption 5 a reasonable simplification for simulation due to the trivial evaporation effects.

The whole duration time for droplet generation and transport is short (less than 200 micro seconds). Assumption 6 is based on the fact that the movement in vertical direction is negligible compared with the movement in horizontal direction. The effect of gravity can be estimated by the Bond number.

$$Bo = \frac{\Delta\rho g L^2}{\sigma} \quad (5)$$

Where:

$\Delta\rho$  is the difference in density of the two phases,

$g$  is the gravitational acceleration,



$L$  is the characteristic length,

$\sigma$  is the surface tension.

In our simulation cases, the Bo number is significantly small due to the infinitesimal characteristic length, therefore we could neglect the effects of gravity.

These assumptions and simplifications would be validated in Chapter 5, compared with existing experimental results.

### 3.2 Model and Computational Geometry

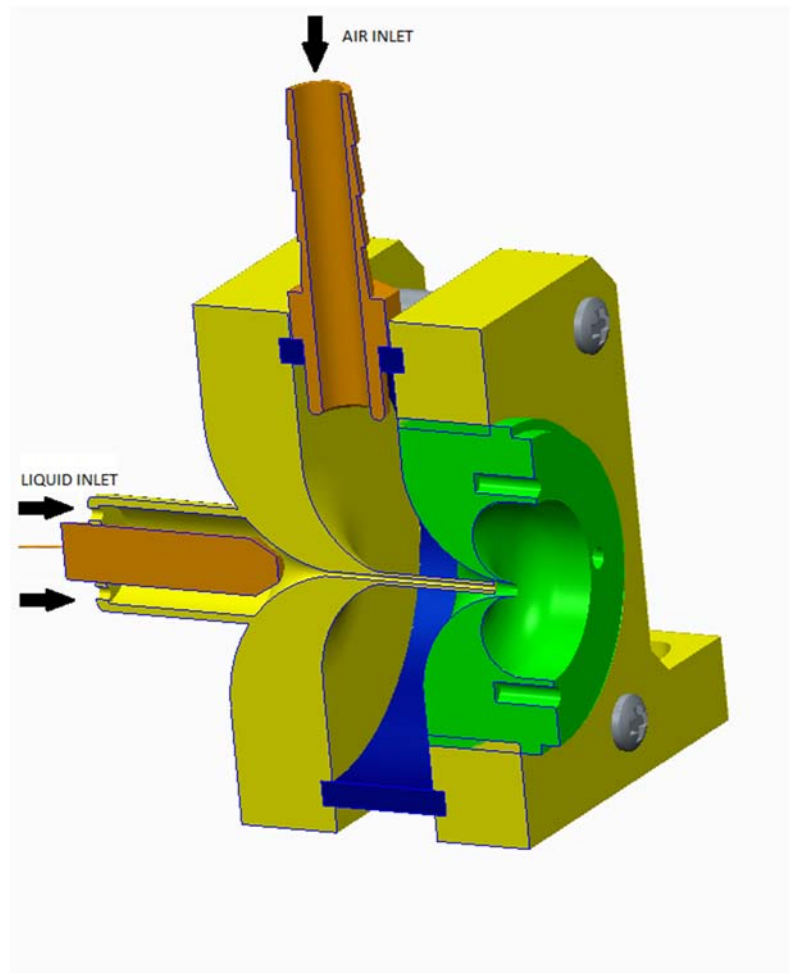


Figure 3.1 Print-head Model

Figure 3.1 displays a view of the Model of the piezo-electric actuated print-head.

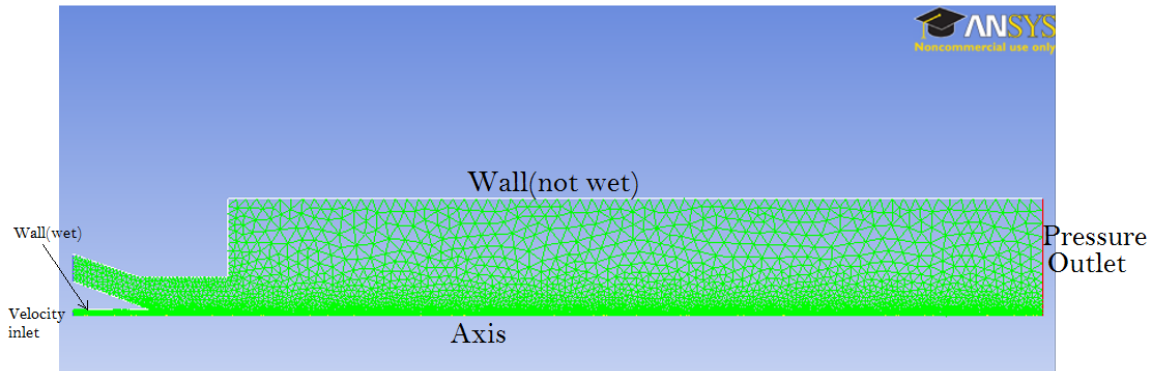


Figure 3.2 Computational Geometry and Grid

Figure 3.2 presents an overall view of the computational geometry and mesh. The diameter of the velocity inlet is variable (30  $\mu\text{m}$ , 40  $\mu\text{m}$ , 50  $\mu\text{m}$ ). The total length of the calculating regime is 2.5mm. The regime close to axis is refined to upgrade the accuracy of droplet generation and transport. The finest grid size employed is 2.5 micron in size. The coarsened mesh that is remote from axis helps to reduce to total grids. The total of 54,366 cells were used for calculation in this project. Typical time steps used were in the range of  $10^{-8} - 10^{-7}$  s.

### 3.3 Governing Equations

In this section, we present the governing equations that describe the droplet generation process. Droplet generation can be treated as a multi-phase (liquid and gas) flow in micron-size geometry.

#### 3.3.1 Basic Conservation Equations

A set of unsteady continuity and Navier-Stokes equations are solved throughout the domain, and the resulting velocity field is shared among the phases. The equations of mass and momentum conservation can be written as follows:

$$\frac{\partial \rho}{\partial t} + \nabla \cdot (\rho \vec{v}) = 0, \quad (6)$$

$$\frac{\partial}{\partial t} (\rho \vec{v}) + \nabla \cdot (\rho \vec{v} \vec{v}) = -\nabla p + \nabla \cdot [\mu (\nabla \vec{v} + \nabla \vec{v}^T)] + \rho \vec{g} + \vec{F}, \quad (7)$$

Here,  $\vec{v}$  is the fluid velocity vector and  $\vec{v} = (u, v, w)^T$ ,  $\rho$  is the fluid density,  $p$  is pressure,  $\mu$  is the fluid's dynamic viscosity,  $\vec{F}$  is a source of momentum, and  $\vec{g}$  is the gravitational force, which is neglected.

One limitations of the shared-fields approximation is that in cases where large velocity differences exist between the phases, the accuracy of the velocities computed near the interface can be adversely affected. In our simulation cases, the velocity difference is in reasonable bounds.

### 3.3.2 Initial and Boundary Conditions

The partial differential equations should be started from an initial condition  $\vec{v} = \vec{v}_0(\vec{x})$ , where  $\vec{x} = (x, y, z)^T$  with  $\nabla \cdot \vec{v}_0(x) = 0$  (divergence-free mass-conserving field).

For the solid zones, non-slip boundary conditions are imposed. The liquid velocity at the wall boundary is set to zero.  $\vec{v}_{wall} = \vec{0}$ .

For the inlet and outlet, open boundary conditions are imposed that permit flow to enter and exit the solution domain. The inlet boundary is set as velocity inlet boundary to define the velocity and scalar properties of the flow at inlet. In this simulations, the total pressure is not fixed but will rise (in response to the computed static pressure) to

whatever value is necessary to provide the prescribed velocity distribution. In this case, the normal component of velocity profile is prescribed by UDF (User defined function) which changes with square wave or sinusoidal wave. At the outlet, a pressure outflow boundary conditions is used to model flow exits where the value of the specified static pressure is set as atmospheric pressure. This pressure is only used while the flow is subsonic. If the flow becomes locally supersonic, the specified pressure will no longer be used, pressure will be extrapolated from the flow in the interior. After all, for this low-speed flow, the specified outlet pressure should be used.

### 3.3.3 Multi-Phase Flow Equations and Volume of Fluid (VOF) model

The Eulerian-Eulerian multi-phase approach for modeling droplet generation is employed in these cases. Although this inhomogeneous Eulerian-Eulerian model is slightly more computational intensive than the homogeneous case, it was preferred due to its intrinsic flexibility.

First, we denote the two phases of fluid using lowercase Greek letters  $\alpha$  and  $\beta$ .

Generally, a quantity subscribed with  $\alpha$  or  $\beta$  describes the value of the quantity for that particular phase. Volume fraction of  $\alpha$  is denoted  $r_\alpha$ . Therefore, the volume  $V_\alpha$  occupied by phase  $\alpha$  in a small volume  $V$  around a point of volume fraction  $r_\alpha$  is given by:

$$V_\alpha = r_\alpha V \quad (8)$$

It is important to distinguish between the material density and the effective density of a fluid  $\alpha$ . The material density,  $\rho_\alpha$ , is the density of the fluid only if it is the only phase present here. The effective density is then defined as:

$$\tilde{\rho}_\alpha = r_\alpha \rho_\alpha \quad (9)$$

And the mixture density is given by:

$$\rho_m = \sum_\alpha \rho_\alpha r_\alpha \quad (10)$$

The total pressure in a multi-phase simulation is defined as:

$$P_{tot} = P_{stat} + \frac{1}{2} \sum_\alpha r_\alpha \rho_\alpha U_\alpha^2 \quad (11)$$

Which is used for both compressible and incompressible flow.

VOF is a numerical method to track the shape and locate position of the fluid-fluid interface. Through solving a single set of momentum equations and tracking the volume fraction of each of the fluids in the domain, VOF models two or more immiscible fluids. VOF model have wide applications, which include jet break-up, motion of large bubbles in a liquid, motion of liquid after a dam break, steady or transient tracking of any liquid-gas interface, etc.

In general, VOF model is employed to solve time-dependent transient problems. For every additional phase introduced in the flow, a variable is needed to denote the volume fraction of the phase in the computational cell. In the control volume, the sum

of each volume fraction equals one. Thus the fields for all variables and properties are shared by the phases and represent volume-averaged values. And the variables and properties in any domain are representative of a mixture of the phases determined by the volume fraction values. That is to say, for instance, we specify the volume fraction of the  $q_{th}$  fluid as  $\alpha_q$ , then the following conditions are simply expressed as:

$\alpha_q = 0$  : The domain is empty of the  $q_{th}$  fluid.

$\alpha_q = 1$  : The domain is full of the  $q_{th}$  fluid.

$0 < \alpha_q < 1$  : The domain contains the interface between the  $q_{th}$  fluid and other fluids.

With the value of  $\alpha_q$ , the properties and variables can be calculated out at each control volume.

The tracking of the interface between two phases is completed by solving a mass conservation equation for the volume fraction of one or more phases. The equation is as following for  $q_{th}$  fluid:

$$\frac{1}{\rho_q} \left[ \frac{\partial}{\partial t} (\alpha_q \rho_q) + \nabla \cdot (\alpha_q \rho_q \vec{v}_q) \right] = S_{\alpha_q} + \sum_{p=1}^n (\dot{m}_{pq} - \dot{m}_{qp}) \quad (12)$$

Where  $\dot{m}_{pq}$  is the mass transfer from phase p to phase q.  $\dot{m}_{qp}$  is the mass transfer from phase q to phase p. Generally, the source term,  $S_{\alpha_q}$ , on the right-hand side is zero.

Only the volume fraction for the secondary phase fluid be solved. And the volume fraction of the primary phase fluid can be calculated by the following equation:

$$\sum_{q=1}^n \alpha_q = 1 \quad (13)$$

## Chapter 4 CFD Simulation Results Analysis

Upon the application of positive pressure charge to the print-head actuator, the fluid starts to flow out of the nozzle. Kinetic energy is transported to fluid outside orifice with the fluid flow. Drop-on-demand droplet generation is significantly influenced by nozzle properties and actuation wave characteristics, including nozzle size, contact angle of nozzle interior wall, actuation frequency, wave peak-to-valley ratio, wave shape. In this section, we discussed the influence from these parameters by numerical simulation.

Simulations were performed on a DELL workstation. This workstation consists of 12 Intel(R) Xeon(R) 2.67 GHz central processors, 48GB of RAM, and dual 250GB Ultra 320 SCSI HDs. ANSYS FLUENT 14.0 was found to be a suitable commercial software for this high-speed two-phase flow calculation. ANSYS FLUENT 14.0 provided a full multiphase coupled solver where all velocities, pressure correction and volume fraction are solved simultaneously. The typical time steps for FLUENT solver were of the order of  $10^{-8}$  s and a typical run consisted of  $1\sim 2\times 10^{-4}$  s (100~200 $\mu$ s of operation time). A general required time to complete one case is about 9 hours. The viscosity of the liquid we used is  $0.1003 \text{ kg} / \text{m} - \text{s}$ , about 100 times of pure water. The surface tension of the liquid we used is  $68.5 \text{ dyn} / \text{cm}$ , lightly smaller than pure water.

### 4.1 Influence of Nozzle Size on DOD Droplet Generation

At the heart of an ink jet printer are a large number of high-precision microscopic nozzles which eject ink onto the paper. These nozzles are typically of the order of 10 microns in diameter (generally 30-80 microns).



In our research work, we performed the reproducible simulations of the ejection process for three nozzles of different diameter (30 $\mu\text{m}$ , 40 $\mu\text{m}$ , 50 $\mu\text{m}$ ) to study the influence of nozzle size on high viscosity droplet generation and break-up process. The actuation frequency is set as 60 kHz. And the simulation time is  $1 \times 10^{-4} \text{ s}$  (100 $\mu\text{s}$ ). To guarantee the liquid has equal kinetic energy per volume, we specify the three cases operated under the same velocity and neglect the different droplets size. In general, the droplet size is 10~20% larger than the nozzle size, depending on the actuation wave form.

In Figure 4.1, images shows the droplet generation process of the high viscous liquid driven by an actuation initial velocity of 13.89 m/s. The droplet ejected from 30  $\mu\text{m}$  nozzle is slightly lower than that from 40  $\mu\text{m}$  may be due to the dissipation of kinetic energy. Droplet from 30  $\mu\text{m}$  diameter nozzle has smaller kinetic energy than that from

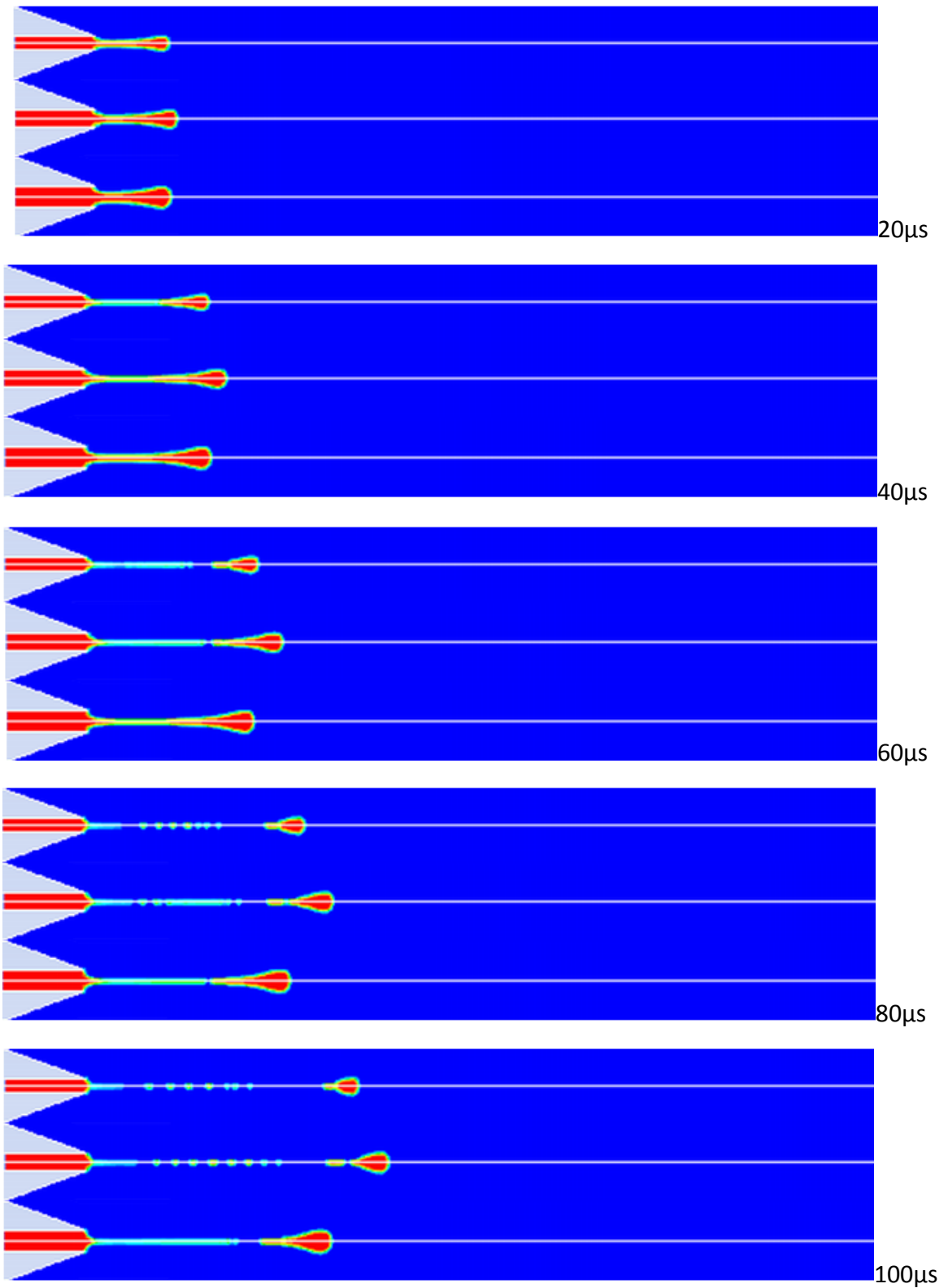


Figure 4.1 Droplet generation of high viscous liquid with viscosity  $0.1003 \text{ kg} / \text{m} - \text{s}$ .  
 From up to bottom on each figure: nozzle size =  $30 \text{ }\mu\text{m}$ ,  $40\mu\text{m}$ ,  $50\mu\text{m}$ .

40  $\mu\text{m}$  diameter nozzle. During the time interval from 40  $\mu\text{s}$  to 100 $\mu\text{s}$ , the droplet from 50  $\mu\text{m}$  diameter nozzle becomes obviously slower than the droplets in the other two cases, even though it has the most kinetic energy. It is because larger nozzle diameter result in longer ligament. The ligament is formed by the liquid between primary droplet and the interior liquid in nozzle. If we treat pure water as a baseline, when the viscosity of liquid increase, the surface tension would decrease. Thus for high viscous liquid, surface tension is not large enough to break up the ligament earlier. Only when the primary droplet travels far from the orifice, the limited volume ligament becomes smaller and smaller, break-up happens with the help of Rayleigh Instability and possible ambient perturbation.

At 40  $\mu\text{s}$  and after, we can find that the 50  $\mu\text{m}$  nozzle case has obvious thicker ligament than the 30  $\mu\text{m}$  and 40 $\mu\text{m}$  nozzle cases. Large nozzle size lead to bigger and longer ligament. Ligament, at first, consume the liquid kinetic energy. And after break up from primary droplet, ligament would unceasingly collapse into a great deal of satellite droplets, which are not desired. Too many satellite droplets directly influence the print quality if they do not hit on the same spot as primary droplet.

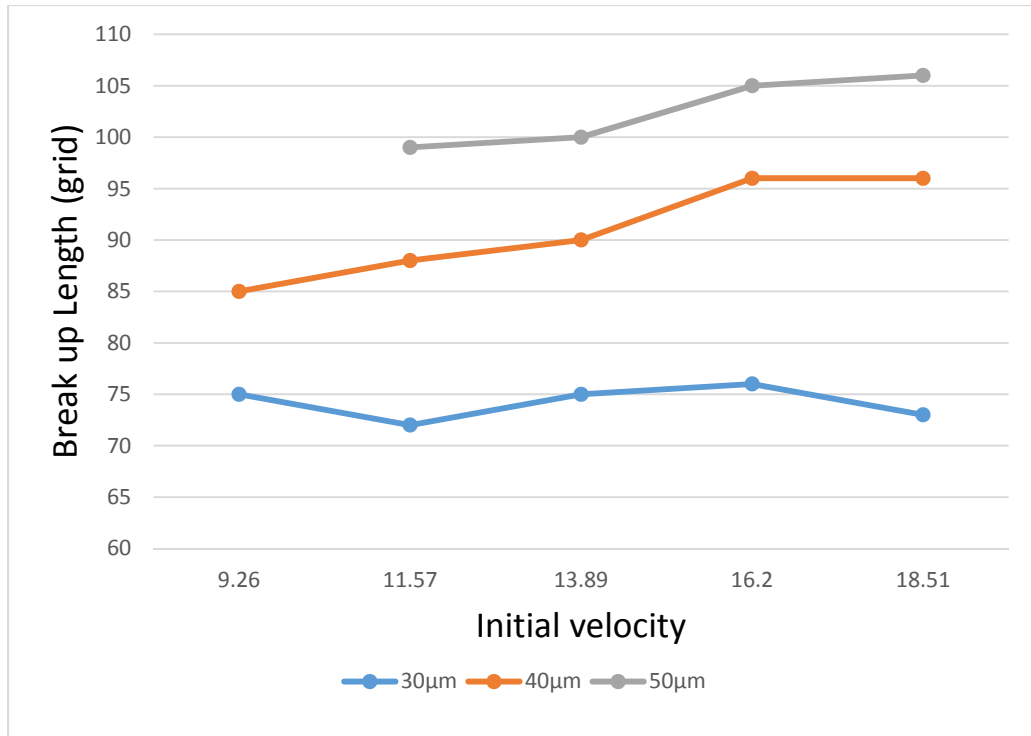


Figure 4.2 Break-up Length with different nozzle diameter for a series of initial ejection velocity

Figure 4.2 shows for a series of different initial ejection velocity cases, break-up length varies with the nozzle diameter. We find that the break-up length increase with the increasing nozzle diameter. The longer the break-up length is, the more kinetic energy is dissipated by stretching liquid. This also helps to explain the fast velocity decrease for 50 µm nozzle case. For a specific nozzle diameter, the break-up length varies slightly at different initial velocity. It is hard to conclude how the initial velocity influence the break-up length.

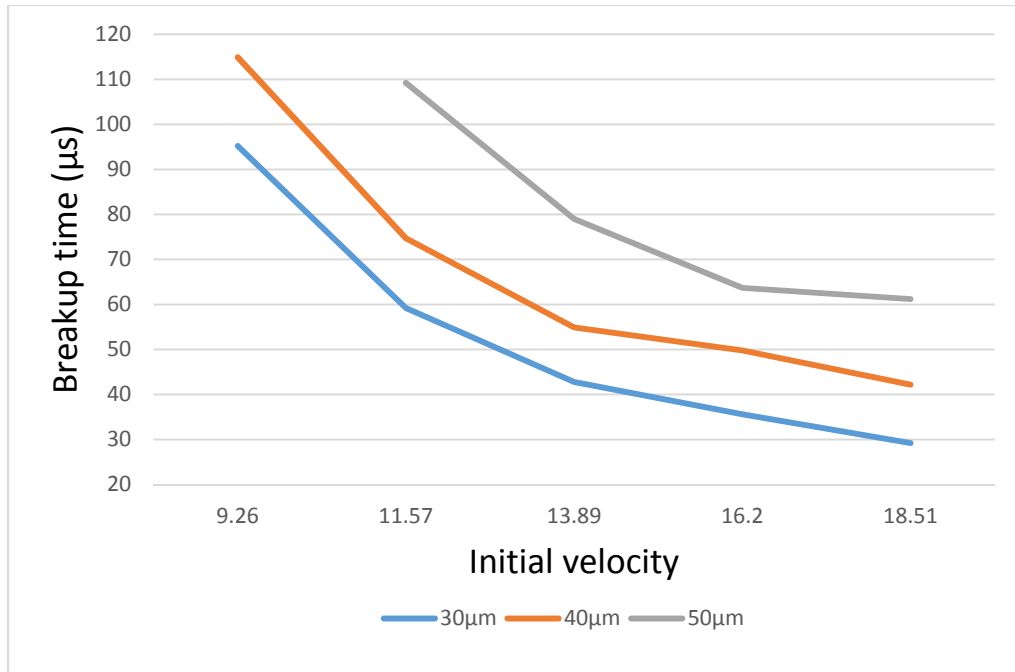


Figure 4.3 Break-up time with different nozzle diameter for a series of initial ejection velocity

In Figure 4.3, with different initial velocity, the break-up time for droplet generation from different nozzle size is shown. At the same initial velocity, the liquid ejected from 50 μm nozzle break up slower than the liquid ejected from smaller nozzle. When the primary droplet is connected with the liquid inside nozzle, it slow down very fast due to the effect of viscosity and ligament stretching. Until the primary droplet break up, the droplet velocity maintains very well, which will be discuss in the next section. This suggests that the earlier the break-up occurs, the earlier the velocity of droplets becomes relatively stable, ignoring the effect of ambient air flow.

#### 4.2 Influence of Actuation Frequency

The actuation frequency have great effect on the droplet generation. At first, for a series frequency of simulations, we should ensure every droplet has the same droplet size as

others. To achieve this requirement, we need to integrate the liquid velocity curve and assign each of the integrals equally. As a result, the droplet generation with higher frequency must possess higher initial velocity. Thus the influence of actuation frequency is also can be treated as the influence of initial velocity. As we mentioned in section 4.1, before the primary droplet break up with ligament, the droplet velocity decrease very fast because before the break-up occurs the kinetic energy dissipated fast due to viscous dissipation.

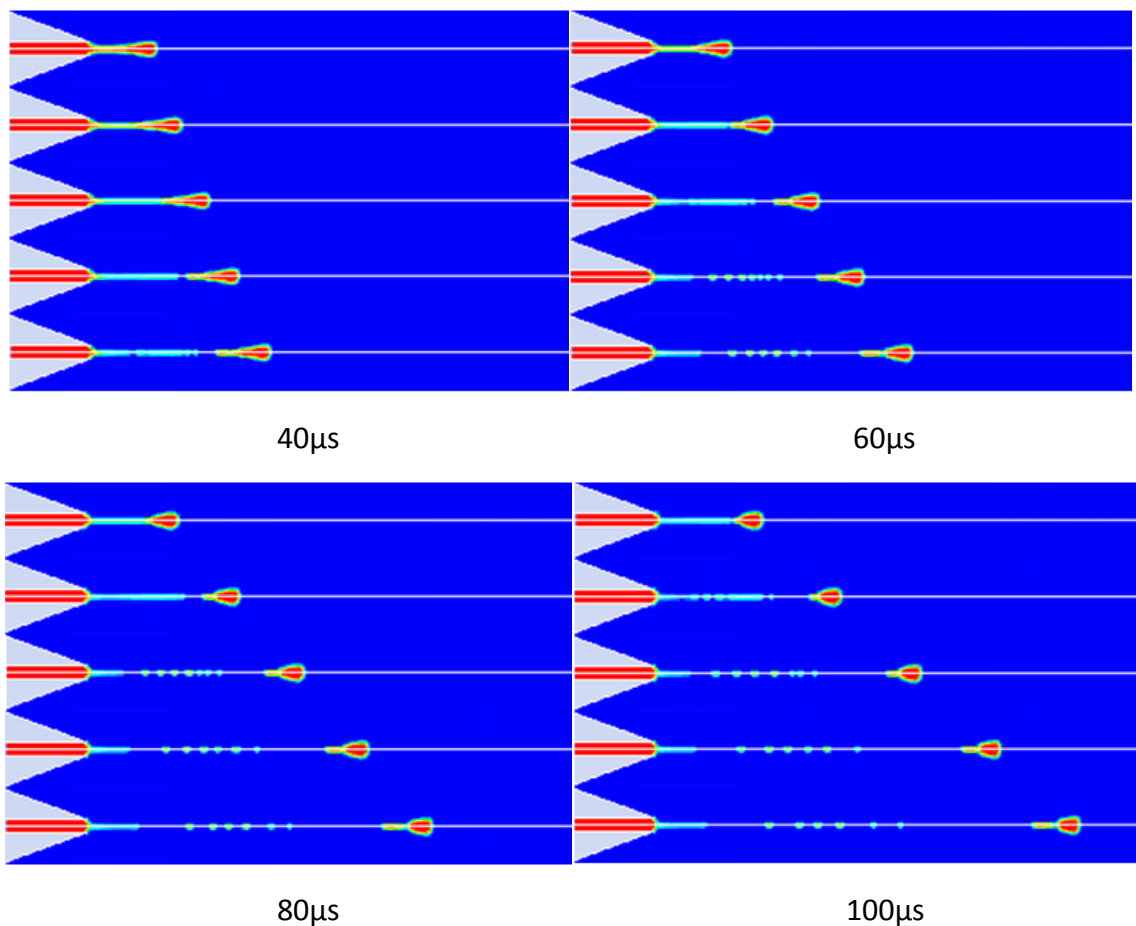


Figure 4.4 Droplet formation of high viscous liquid. Nozzle diameter is 30  $\mu\text{m}$ . In each image, from up to bottom: actuation frequency = 40 kHz, 50 kHz, 60 kHz, 70 kHz, and 80 kHz. Images are presented every 20  $\mu\text{s}$  from 40  $\mu\text{s}$  to 100  $\mu\text{s}$ .



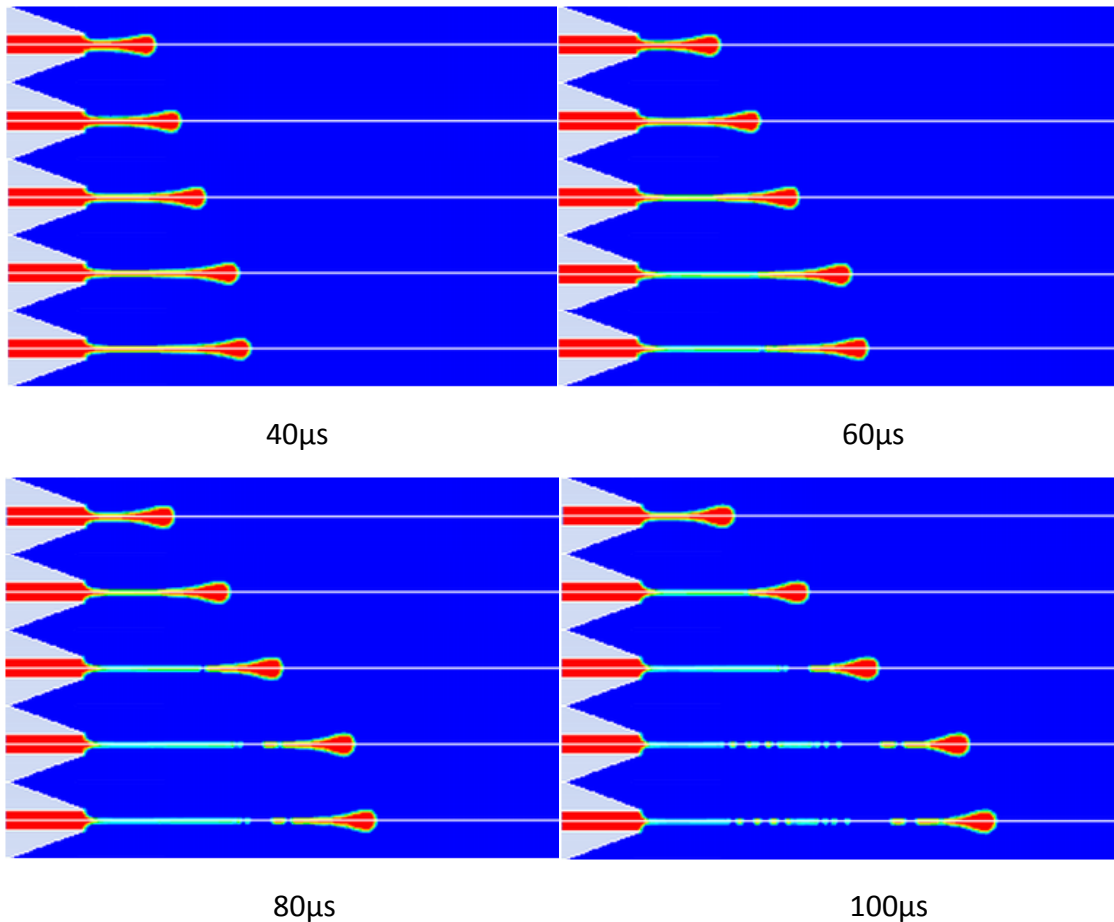


Figure 4.6 Droplet formation of high viscous liquid. Nozzle diameter is 50  $\mu\text{m}$ . In each image, from up to bottom: actuation frequency = 40 kHz, 50 kHz, 60 kHz, 70 kHz, and 80 kHz. Images are presented every 20  $\mu\text{s}$  from 40  $\mu\text{s}$  to 100  $\mu\text{s}$ .

In these three groups of figures (Figure 4.4, 4.5, 4.6), droplet generation of highly viscous liquid at different actuation frequencies are presented. When the actuation frequency is as low as 40 kHz, the liquid ligament can hardly break up. The primary droplet formed after ejecting, however, almost stopped in less than 100  $\mu\text{s}$ . I also attempt to simulate the ejection with a frequency less than 40 kHz, but all tries were failed.



For actuation frequency of 80 kHz, during the time interval between 40  $\mu$ s and 60  $\mu$ s, the liquid ligament begin to get thinner. And during the following 20  $\mu$ s, the ligaments collapse into several satellite droplets. Even though these satellite droplets come from the same ligament, they possess different velocity. The satellite droplets with faster velocity catch up with the primary droplet. The satellite droplets with slower velocity recombine with latter satellite droplets to form a large droplet.

Time	40kHz	50kHz	60kHz	70kHz	80kHz
10 $\mu$ s	7.49	8.65	9.96	11.1	12.5
20 $\mu$ s	3.57	4.92	6.62	8.47	10.4
30 $\mu$ s	2.36	4.17	5.92	7.92	10
40 $\mu$ s	2.05	3.82	5.75	7.66	9.54
50 $\mu$ s	1.64	3.47	5.57	7.37	9.55
60 $\mu$ s	1.52	3.31	5.34	7.02	9.59
70 $\mu$ s	1.56	3.21	5.07	6.7	9.5
80 $\mu$ s	1.54	3.13	4.8	6.5	9.43
90 $\mu$ s	1.54	3.13	4.7	7.09	9.4
100 $\mu$ s	1.6	3.18	4.57	6.66	9.35

Table 4.1 Droplet velocity record for different actuation frequency: 40 kHz, 50 kHz, 60kHz, 70 kHz, and 80 kHz

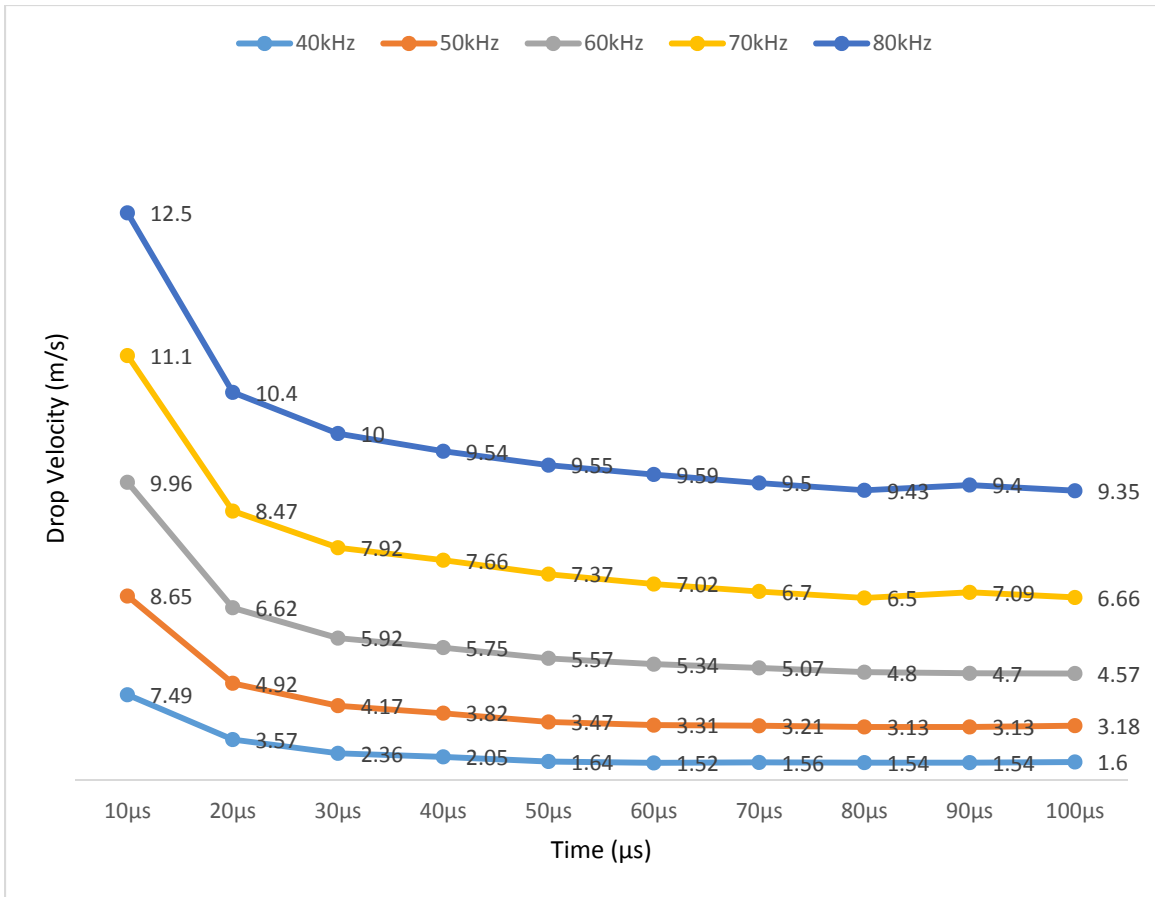


Figure 4.7 Droplet velocity record for different actuation frequency: 40 kHz, 50 kHz, 60kHz, 70 kHz, and 80 kHz

The droplet velocity decreasing process is shown in Table 4.1 and Figure 4.7. In Figure 4.7, we found the droplet velocity decrease vary fast during the time interval between 0  $\mu$ s and 30  $\mu$ s. On each of the curves, there is a point that the gradient changes notably. This point, in general, is the time the ligament break up with primary droplet. After this point, the droplet velocity tend to more stable than before. The stable fly period is usually desired for droplets to travel long distance. Obviously, high frequency is preferred not only because it is easy to control the hit point but also there is less ambient disturbance during fly. If the droplet fly velocity is not stable, fast droplet may

catch up with slower one and combine. In a result, larger volume droplet slow down and influence the print quality.

#### 4.3 Influence of Actuation Wave Peak-to-Valley Ratio

We generally use sinusoidal wave and square wave as the DOD actuation wave form, which will be investigated in next section 4.4. In this section, we only discuss the time ratio of the wave peak and wave valley for square wave. In each case, we simulation is about generating three successive droplets with the frequency of 60 kHz. Four peak-to-valley ratios are selected to simulate: 1:1, 1:2, 1:3, and 1:4 as shown in Figure 4.8. Each of the four cases has the same initial velocity, 13.89 m/s.

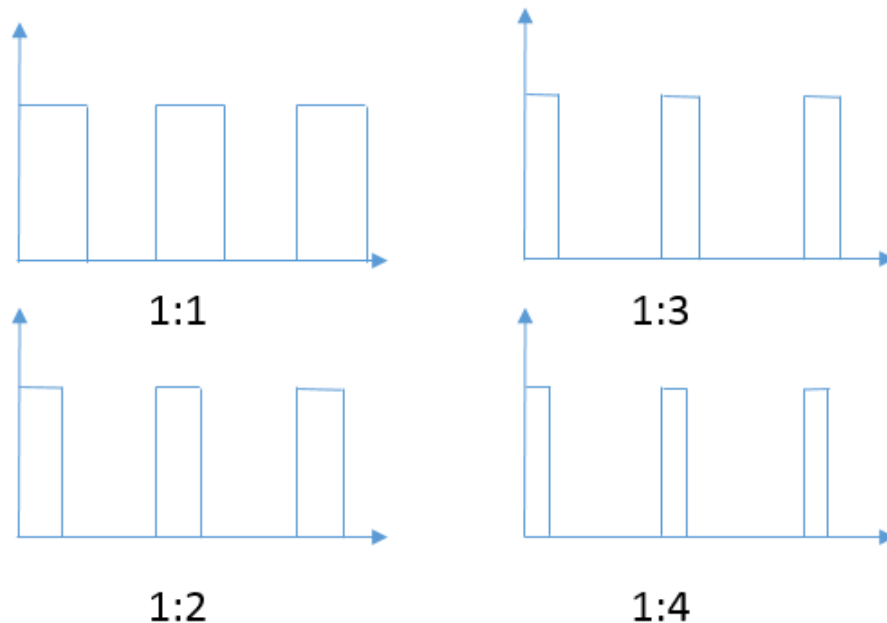


Figure 4.8 Four selected peak-to-valley ratio wave form

The interval time between two consecutive actuation signal increase as the peak-to-valley ratio decrease from 1:1 to 1:4. After one actuation, the pressure wave need enough time to be completely damped by viscous dissipation before the next pressure

pulse is applied. This effect is significant for low viscous fluid droplet generation. However in our high viscous liquid simulations, the time interval influences less significantly.

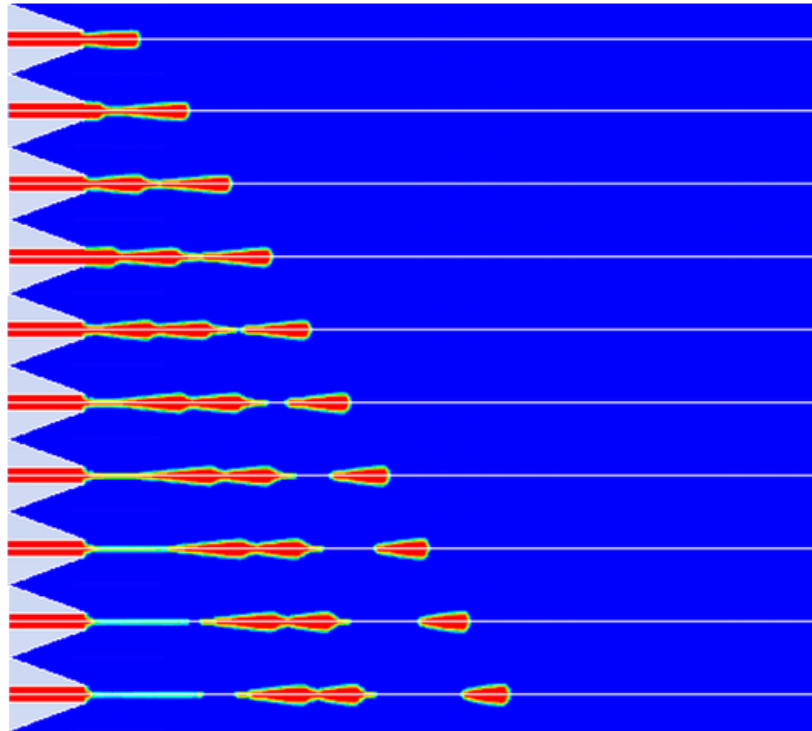


Figure 4.9 Three DOD droplet generation with a peak-to-valley ratio 1:1. From top to bottom, images begin from 0  $\mu\text{s}$  to 100  $\mu\text{s}$ . Time interval is 10  $\mu\text{s}$

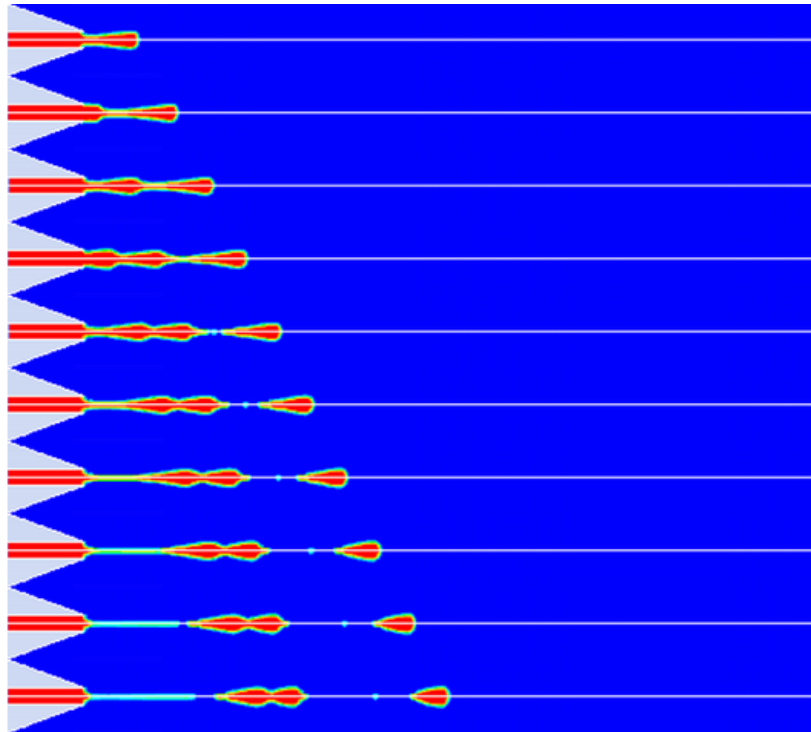


Figure 4.10 Three DOD droplet generation with a peak-to-valley ratio 1:2. From top to bottom, images begin from 0  $\mu\text{s}$  to 100  $\mu\text{s}$ . Time interval is 10  $\mu\text{s}$

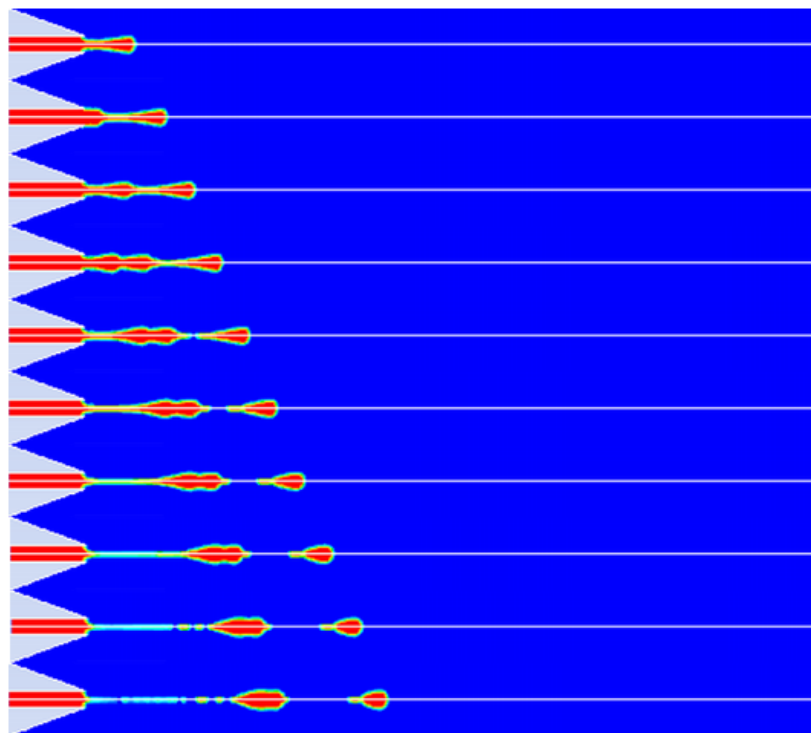


Figure 4.11 Three DOD droplet generation with a peak-to-valley ratio 1:3. From top to bottom, images begin from 0  $\mu\text{s}$  to 100  $\mu\text{s}$ . Time interval is 10  $\mu\text{s}$

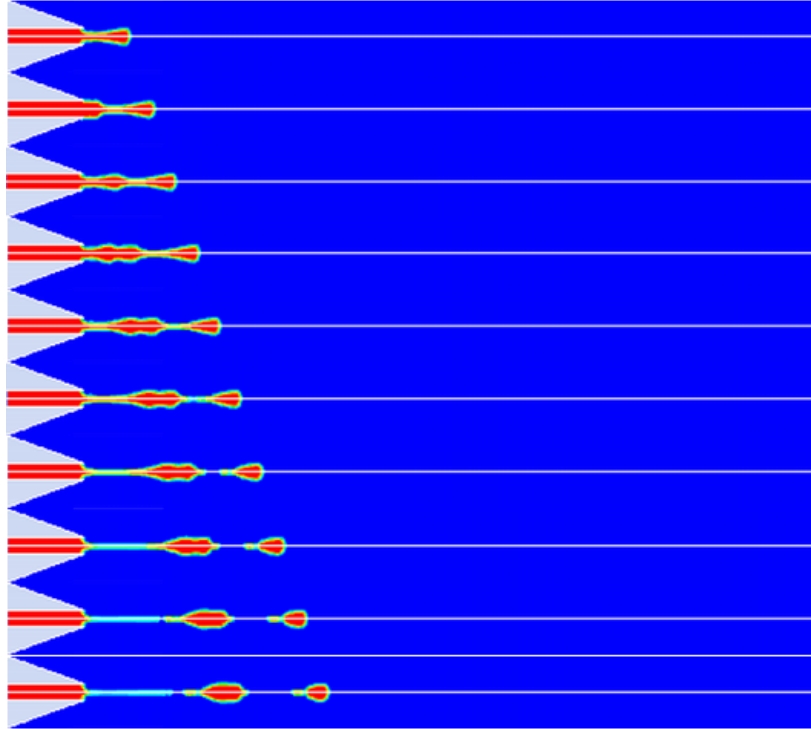


Figure 4.12 Three DOD droplet generation with a peak-to-valley ratio 1:4. From top to bottom, images begin from 0  $\mu\text{s}$  to 100  $\mu\text{s}$ . Time interval is 10  $\mu\text{s}$

From Figure 4.9 to Figure 4.12, images of DOD droplet generation of high viscous liquid at different peak-to-valley actuation wave form are shown. Comparing these images we can find, as the peak-to-valley ratio decrease, in other words as the interval time between two actuation pulse increase, the last two droplet tend to combine together. This result is totally different from the former results regarding low viscous fluid. This is because as the viscosity incredibly increase to as high as 100 times of water, the energy dissipation effect is getting faster, but the deformation of the liquid inside nozzle is much slower, even still for some kind of Non-Newtonian fluids. Thus when the third droplet begins to outflow, the second droplet is still hold by the high viscous fluid inside the nozzle.

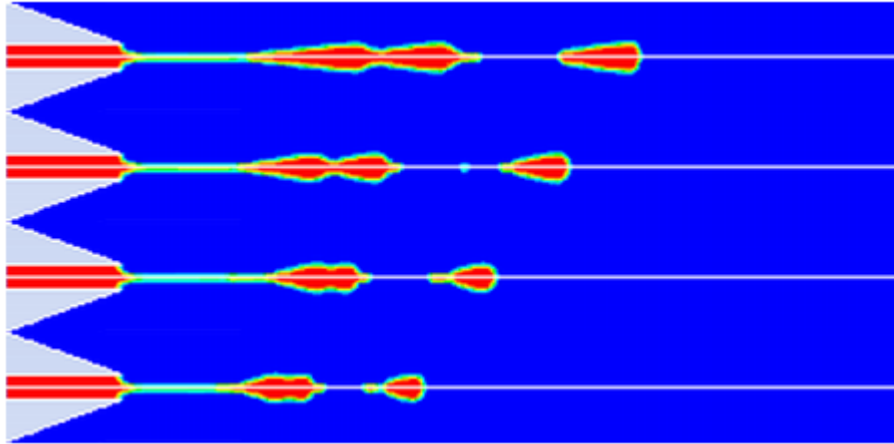


Figure 4.13 Images of DOD droplet generation of different peak-to-valley ratio. Images are recorded at  $80 \mu\text{s}$ . From top to bottom on each image, peak-to-valley ratio = 1:1, 1:2, 1:3, and 1:4. Actuation frequency = 60kHz.

As the wave peak-to-valley ratio decrease from 1:1 to 1:4, the droplets velocity decreases slightly as Figure 4.13 shows. Because with the decreasing of the peak part of the actuation wave, the kinetic energy of each liquid column, which forms one primary droplet and corresponding satellite droplets, is reduced. In addition, for these cases, the nozzle diameter, surface tension and viscosity are fixed as the same. Thus the viscous damping effects, which determined by above characters, are identical with each other.

#### 4.4 Influence of Actuation Wave Shape

In this section, we investigate the effects of the shape of the actuation wave form. As we mentioned in last section, most DOD print-head use two types of actuation wave shape: square wave and sinusoidal wave due to the intrinsic characteristic of piezo-electric actuator and thermal actuator.

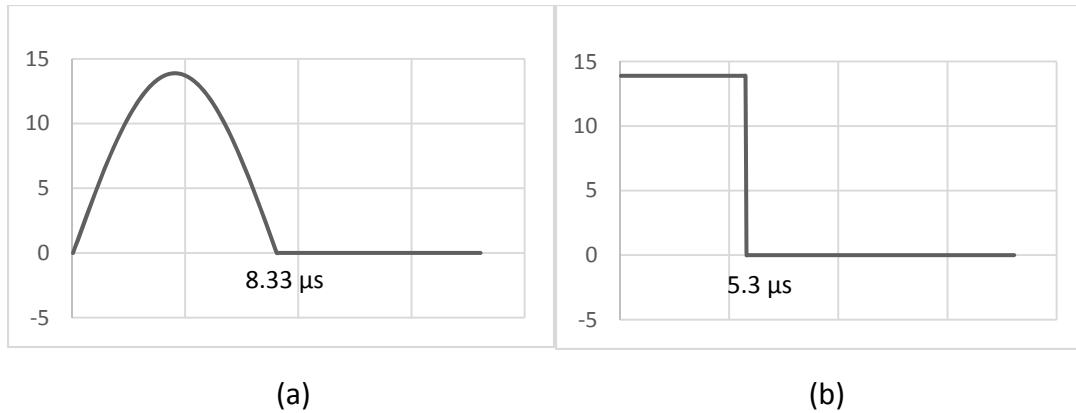


Figure 4.14 Sinusoidal and square wave form. X axis is the elapsed time, Y axis is the velocity of liquid column before the formation of droplet

Figure 4.14 depicts the two shape types of actuation waveform. Figure 4.14 (a) shows the sinusoidal wave shape with the frequency of 60 kHz. The period of this wave is  $16.66 \mu\text{s}$ . As we effaces the negative part of pulse, the second half of this period is equal to zero. At this part, the print-head is under the refilling process. Liquid is refilled from a large volume reservoir. The pressure inside the nozzle is slightly positive but not large enough to push out the liquid. Figure 4.14 (b) shows the square wave shape with the same frequency as Figure 4.14 (a). We need to ensure the integral of these two shape identical, in other words, we should guarantee the uniform droplets volume for these two cases. Thus the positive pulse part of the square wave only last  $5.3 \mu\text{s}$ , and the refilling process follows.



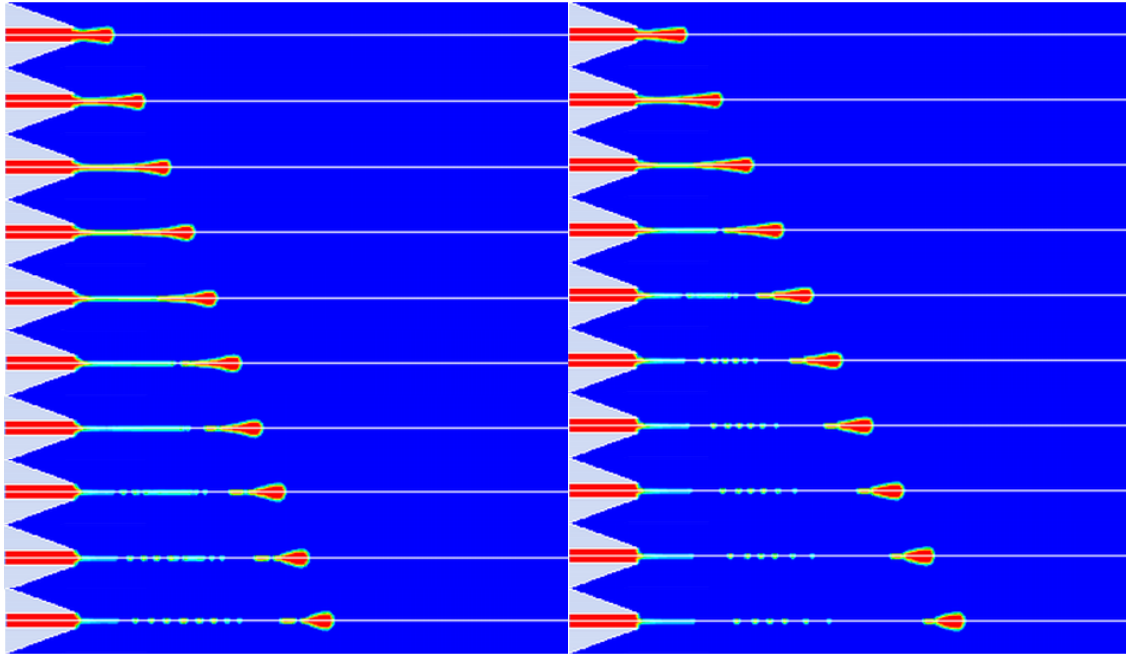


Figure 4.15 Simulation results of droplet generation of (a) sinusoidal wave and (b) square wave. Each of image (a) and (b), from top to bottom, begins when liquid emerges from the nozzle and shown for every  $10 \mu\text{s}$  through  $100 \mu\text{s}$ .

Figure 4.15 shows the droplet generation process driven by sinusoidal wave actuation (a) and square wave actuation (b). For these two cases, droplets possess the same Reynolds number, Weber number, and Ohnesorge number, therefore they have identical kinetic energy, surface tension and viscous dissipation effects. Comparing the two images, we found the droplet actuated by square wave break up earlier than the droplet driven by sinusoidal wave. And thus the droplets in (b) is a little faster than that in (a) which hit the substrate later. At  $30 \mu\text{s}$ , the ligament in (a) is obvious thicker than the ligament in (b). From  $40 \mu\text{s}$  to  $100 \mu\text{s}$ , we found the ligaments collapsed into satellite droplets. And therefore case (a) has more satellite droplets than case (b). At  $60 \mu\text{s}$ , the tail of the primary droplet in case (a) is longer than the tail in case (b). This indicates that, at last, the primary droplet of case (a) will be slightly larger than the primary

droplet of case (b), because the tail of a droplet will finally shrink into the droplet due to the help of surface tension.

#### 4.5 Influence of Nozzle Inner Wall Contact Angle

In this section, we discussed the influence due to the different wettability of the nozzle inner wall. The wettability is determined by the material property of the nozzle. And the contact angle is a feature to show this property. Contact angle quantifies the wettability of a solid surface and a liquid. Contact angle ranges from the so-called advancing (maximal) contact angle to the receding (minimal) contact angle.

In our simulation, we studied the contact angle of  $0^\circ$ ,  $45^\circ$ ,  $90^\circ$ ,  $135^\circ$ , and  $180^\circ$ . Ejection velocity is 3m/s. An air flow is added to help the liquid column break up and accelerate.

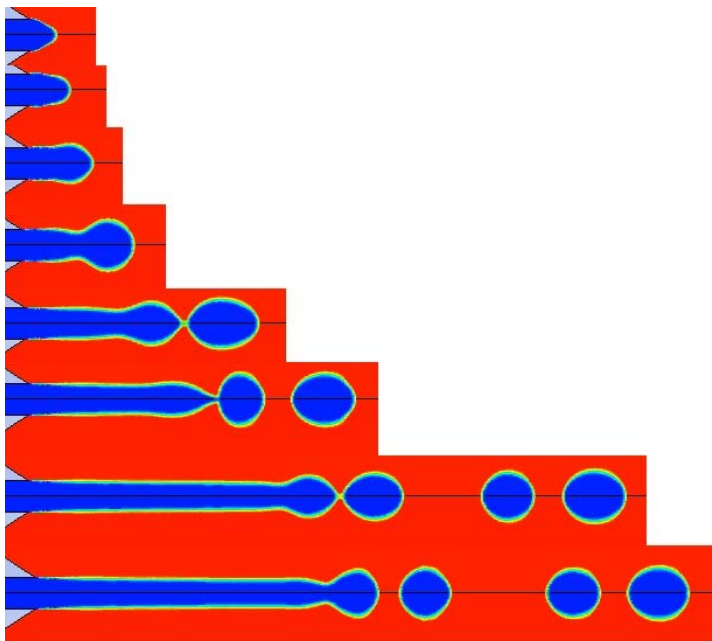


Figure 4.16 Droplet generation with the nozzle wall contact angle of  $0^\circ$ . From top to bottom, the time for each image is:  $8.4 \mu\text{s}$ ,  $17.7 \mu\text{s}$ ,  $37.3 \mu\text{s}$ ,  $75.6 \mu\text{s}$ ,  $138.0 \mu\text{s}$ ,  $181.0 \mu\text{s}$ ,  $280 \mu\text{s}$ ,  $300 \mu\text{s}$ .

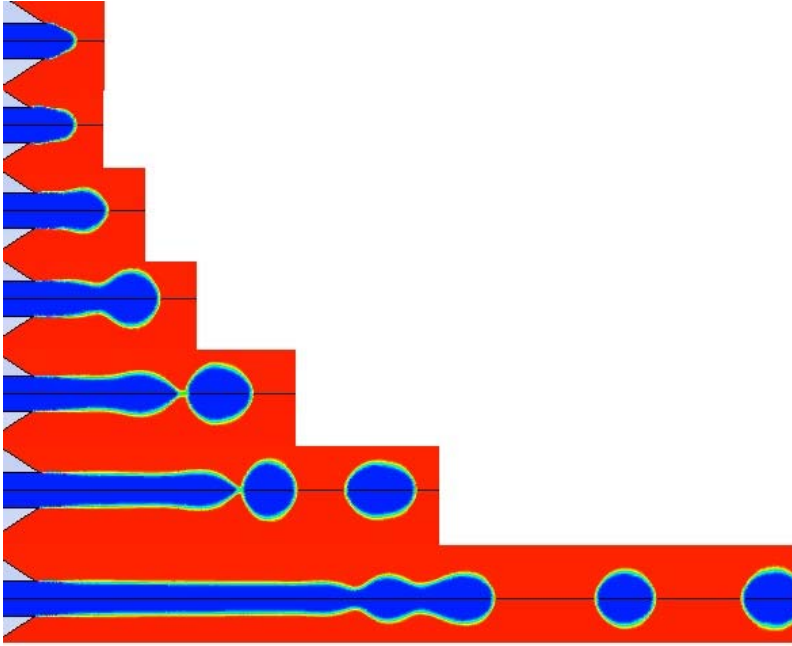


Figure 4.17 Droplet generation with the nozzle wall contact angle of  $45^\circ$ . From top to bottom, the time for each image is:  $8.4 \mu\text{s}$ ,  $17.7 \mu\text{s}$ ,  $37.3 \mu\text{s}$ ,  $75.6 \mu\text{s}$ ,  $138.0 \mu\text{s}$ ,  $181.0 \mu\text{s}$ ,  $280 \mu\text{s}$ ,  $300 \mu\text{s}$ .

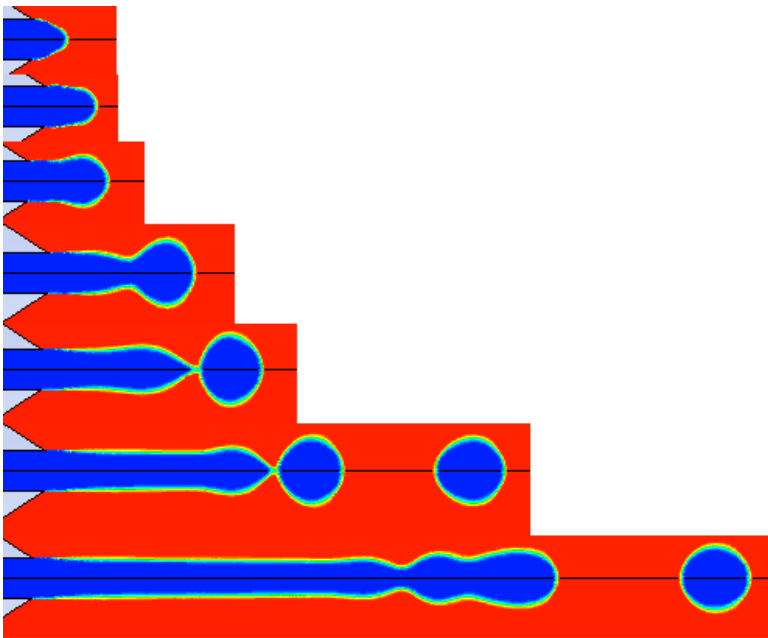


Figure 4.18 Droplet generation with the nozzle wall contact angle of  $90^\circ$ . From top to bottom, the time for each image is:  $8.4 \mu\text{s}$ ,  $17.7 \mu\text{s}$ ,  $37.3 \mu\text{s}$ ,  $75.6 \mu\text{s}$ ,  $138.0 \mu\text{s}$ ,  $181.0 \mu\text{s}$ ,  $280 \mu\text{s}$ ,  $300 \mu\text{s}$ .

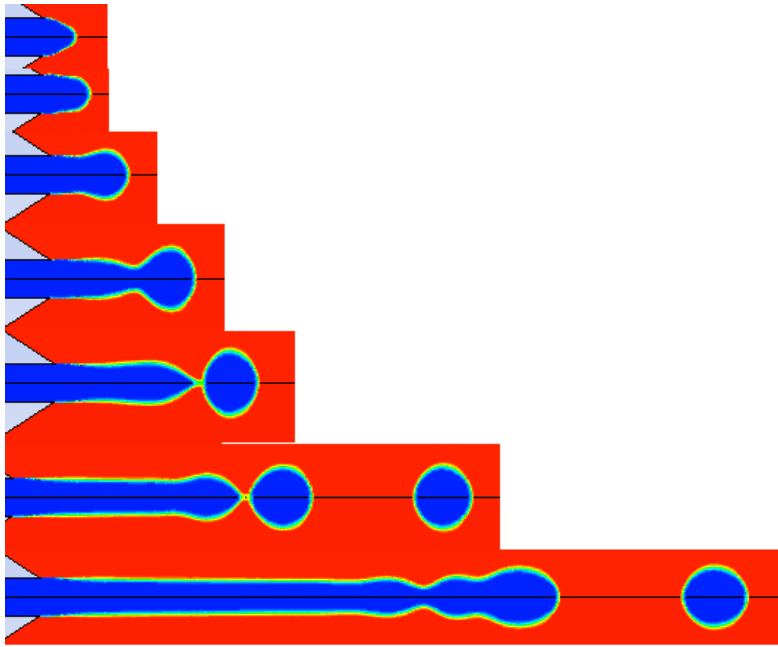


Figure 4.19 Droplet generation with the nozzle wall contact angle of  $135^\circ$ . From top to bottom, the time for each image is:  $8.4 \mu\text{s}$ ,  $17.7 \mu\text{s}$ ,  $37.3 \mu\text{s}$ ,  $75.6 \mu\text{s}$ ,  $138.0 \mu\text{s}$ ,  $181.0 \mu\text{s}$ ,  $280 \mu\text{s}$ ,  $300 \mu\text{s}$ .

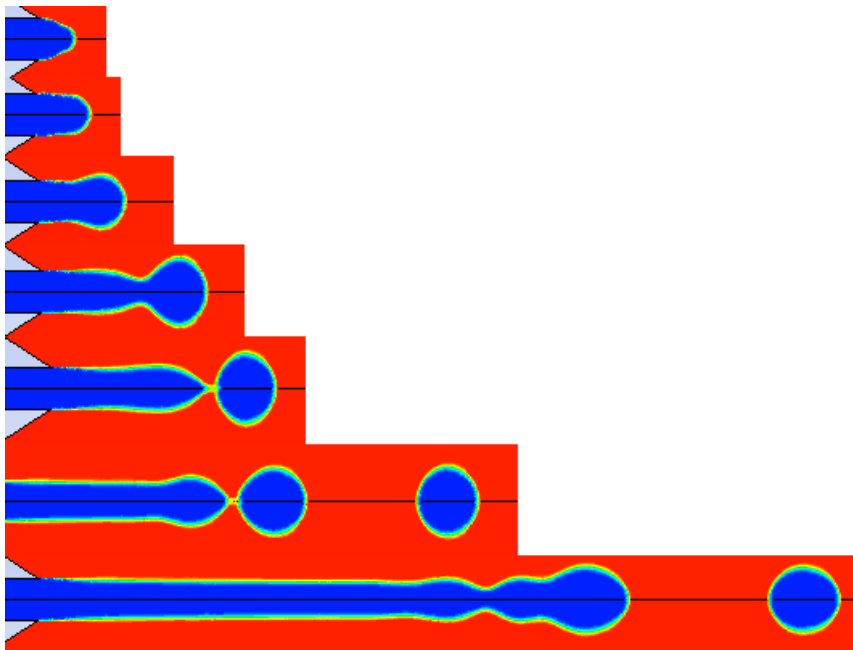


Figure 4.20 Droplet generation with the nozzle wall contact angle of  $180^\circ$ . From top to bottom, the time for each image is:  $8.4 \mu\text{s}$ ,  $17.7 \mu\text{s}$ ,  $37.3 \mu\text{s}$ ,  $75.6 \mu\text{s}$ ,  $138.0 \mu\text{s}$ ,  $181.0 \mu\text{s}$ ,  $280 \mu\text{s}$ ,  $300 \mu\text{s}$ .

As the contact angle increase from  $0^\circ$  to  $180^\circ$ , the liquid column before break up become longer, and the time to obtain the first droplet is getting longer as Figure 4.16 to Figure 4.20 shows. At  $300 \mu\text{s}$ , the nozzle of  $0^\circ$  contact angle has already generated 3 single droplets, however, the nozzle of  $180^\circ$  contact angle generated only 1 droplet.

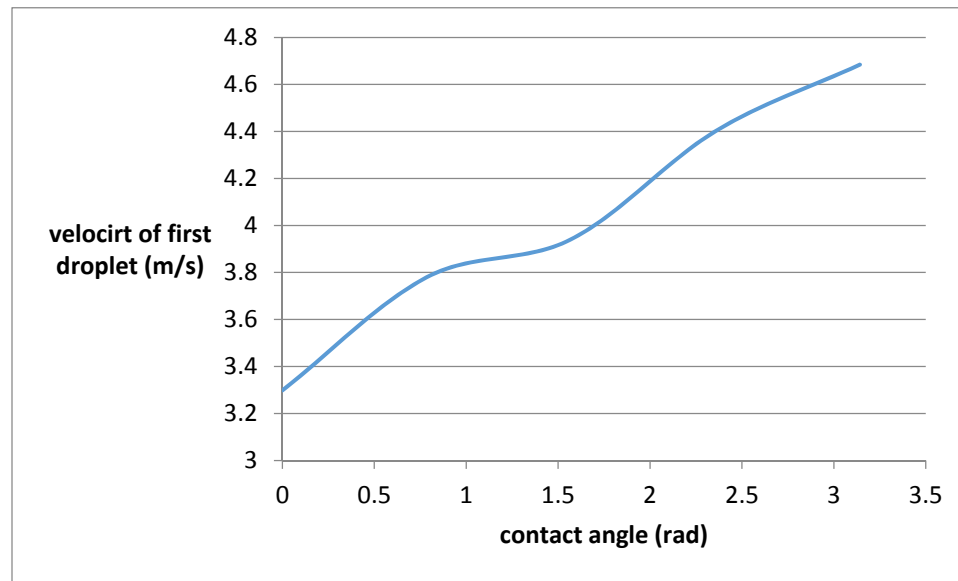


Figure 4.21 The velocity variation of the first droplet with different contact angle.

Figure 4.21 shows with the increasing contact angle, the velocity of the first droplet increases. This is recorded at  $300 \mu\text{s}$ .

#### 4.6 Droplets Transport

After the droplet is fully generated, we should consider the process that droplet travels to hit the substrate. For most inkjet, the droplets travel distance is usually range from 1 cm to 5 cm. However for other applications, such as automotive painting, the droplets travel distance can be extended to 10 cm and even longer. Inkjet works in an environment with stable or still air condition, but some other applications are located in a much more complicated environment even at a place with lateral air flow.

For droplets travels long distance, the deceleration of the droplet is obvious and may cause disaster results. When the droplets ahead decelerate, the latter droplet would hit on the ahead one and combine into one large droplet. Large droplet decelerate even faster. This is shown in Figure 4.22. 12 droplets are generated in this case, however at 85 $\mu$ s, only five droplets remains.

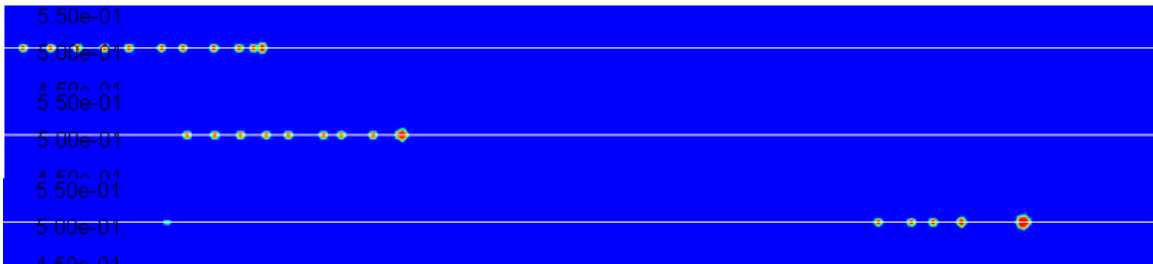


Figure 4.22 Droplet travels long distance without air flow. These 3 images are recorded at time: 30  $\mu$ s, 40  $\mu$ s and 85 $\mu$ s.

For some complex droplet generation applications, a stable air flow along the direction of liquid ejection can be applied to help droplets travels longer distance. In a low velocity air flow condition, droplets travels more stable as shown in Figure 4.23. The distance between two droplets are relatively uniform. Even though the first droplet encroach latter ones but this process is much slower.

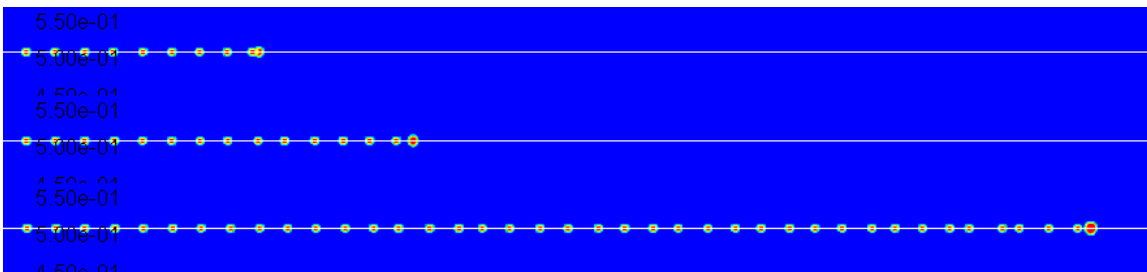


Figure 4.23 A series droplets generation with a right-direction air flow of 5m/s. These 3 images are recorded at time: 30  $\mu$ s, 40  $\mu$ s and 85 $\mu$ s.

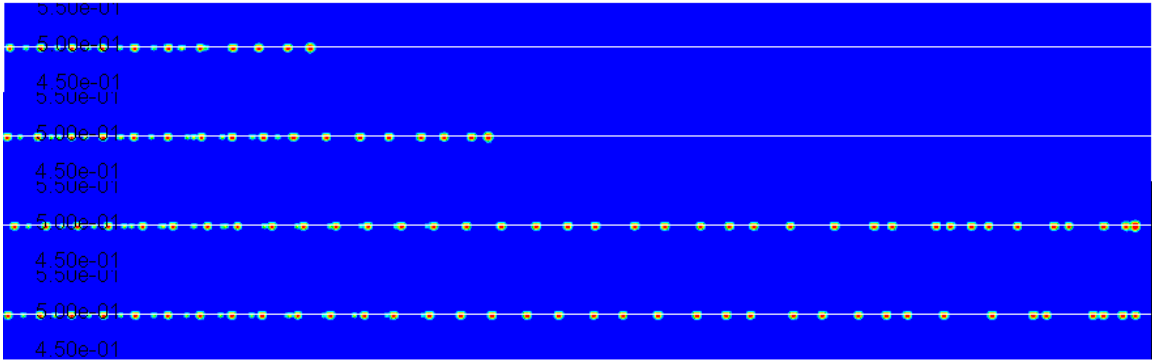


Figure 4.24 A series droplets generation with a right-direction air flow of 15 m/s. These 4 images are recorded at time: 30  $\mu$ s, 40  $\mu$ s, 77 $\mu$ s and 85 $\mu$ s.

Figure 4.24 shows the same droplets generation but with the air flow with higher velocity, 15 m/s. We found in this case, the droplets travels faster than the case in Figure 4.23. But one more problem arises. After certain distance travel, the droplets becomes unstable. The interval space between two droplets is variable violently. One reason to cause this problem might be the air flow condition switch. At first, the air flow is laminar flow, which is desired. But after about 1 cm travel, the air flow velocity increase sharply and the air flow switch to turbulent flow. At this moment, the Reynolds number of the air flow increase to about 2000.

## Chapter 5 Conclusion and Recommendation

In this thesis, a liquid of high viscosity has been used to investigate several effects on DOD droplets generation and transport. The research work is completed by numerical simulation in ANSYS FLUENT 14.0. Through this high-speed calculations, the factors that influence the process of droplet generation and transport are studied.

### 5.1 Summaries and Conclusions

The following conclusions can be drawn from this thesis:

- 1) *Nozzle Size Influence* - Small nozzle size lead to small kinetic energy transmitted to liquid column and thus result to slow droplet velocity. But if the nozzle size is too large, thicker and longer ligament consumes more kinetic energy as well. In addition, large nozzle size bring in more satellite droplets, which should be avoided. Large nozzle size cause longer break up length and longer break up time. As the process before breaking up is an energy consuming procedure, we need to shorten the time of this process so as to increase the energy remaining in droplet.
- 2) *Actuation Frequency Influence* – Simulations on the actuation frequency of 40 kHz, 50 kHz, 60 kHz, 70 kHz, and 80 kHz for the high viscous liquid are reproducible. The volume of each droplet is identical, thus, the initial velocity increase with the increasing actuation frequency. Actuation frequency, lower than or equal to 40 kHz, can hardly produce a single droplet and the liquid stopped in less than 100  $\mu$ s. Actuation frequency above 70 kHz is ideal for



droplet generation of high viscous fluid. At these frequencies, primary droplets break up after 50-60  $\mu\text{s}$ , and stably fly further. Usually, the time point of break-up is the watershed of droplet velocity decreasing sharply and droplet travels relatively stable. High frequency helps to reach this separation point earlier.

- 3) *Actuation Wave Peak-to-Valley Ratio Influence* – Four peak-to-valley ratios are simulated in this thesis, 1:1, 1:2, 1:3, 1:4, and three droplets are generated in each case. With the peak-to-valley ratio decrease, the last two droplets are easier to coalesce. When the peak-to-valley ratio decrease, the energy transmission time decrease as well. Thus the droplets driven by wave peak-to-valley ratio of 1:4 decelerate faster than high peak-to-valley ratio actuation wave, 1:1.
- 4) *Actuation Wave Shape Influence* – Square wave and sinusoidal wave are applied to push out droplets. Square wave actuation would be preferred if the print-head allows. Droplet actuated by square wave break up earlier than that actuated by sinusoidal wave, which means less kinetic energy dissipation. Moreover, the liquid driven by sinusoidal wave forms thicker ligaments, which breaks up into more undesired satellites droplets.
- 5) *Nozzle Inner Wall Contact Angle Influence* – We investigated the contact angle of  $0^\circ$ ,  $45^\circ$ ,  $90^\circ$ ,  $135^\circ$ , and  $180^\circ$ . In the 300  $\mu\text{s}$  simulation time, smaller contact angle generated more droplets. And the nozzle with  $180^\circ$  contact angle produce one complete droplet latest. In addition, as the contact angle increase, the velocity of droplets increases.

6) Droplet Transport – We studied the droplet travel process after break up from liquid inside the nozzle. Air become a very important factor during the transport. Without air flow carrying, the first droplet decelerate fast and coalesce with latter droplets. Finally more than half of the droplets combined together into a large and slow droplet. With the 5 m/s air flow carrying, droplets travels more stable. Only very few droplets coalesce. With a 15 m/s air flow carrying, new problem arises. Air flow turned to turbulent flow from the original laminar flow. This change cause the droplets sequence unstable and the distance between two droplets varies significantly.

## 5.2 Recommendations

The following aspects could be studied to better estimate the droplet generation behaviors.

- 1) In this thesis, we only used circular nozzle. Liquid ejected from other types of cross section may have different results, such as square, regular polygon, etc. Other shapes of cross section may have positive effect on expediting the ligament break up.
- 2) We may find another method to study the actuation frequency influences with fixed initial velocity for different frequencies through scale modeling method.
- 3) We may try many other wave shape as actuation. Such as large positive pulse followed by a small negative pulse, double positive pulse with very small

interval time, one large positive pulse followed by a small positive pulse, one small positive pulse followed by a large positive pulse, etc. When using two pulses in one droplet generation, we can change the peak value ratio as well.

- 4) For the droplet transport carried by air flow, we can change the air inlet direction to avoid the transform from laminar flow to turbulent flow. We can even change the cross section area of the calculating domain to prevent the flow condition transform.

## Appendix

### Liquid Inlet User Defined Function (UDF) Code

```
#include "udf.h"
#include "sg.h"
#include "sg_mphase.h"
#include "flow.h"

#define PI 3.141592654
DEFINE_PROFILE(speed_1000, th, nv)

/* membrane speed - function name */
/* th - thread */
/* nv - variable number */
{
    face_t f;
    real x[ND_ND];
    real f_time = RP_Get_Real("flow-time");

    begin_f_loop (f, th)
    {
        F_CENTROID(x, f, th);
        if (f_time<=8.33e-6 || (f_time>=16.66e-6 && f_time<=24.99e-6)
            || (f_time>=33.32e-6 && f_time<=41.65e-6) || (f_time>=49.98e-6 &&
f_time<=58.31e-6)
            || (f_time>=66.64e-6 && f_time<=74.97e-6) || (f_time>=83.3e-6 &&
f_time<=91.63e-6)
            || (f_time>=99.96e-6 && f_time<=108.29e-6) || (f_time>=116.62e-6 &&
f_time<=124.95e-6)
            || (f_time>=133.28e-6 && f_time<=141.61e-6) || (f_time>=149.94e-6 &&
f_time<=158.27e-6)
            || (f_time>=166.6e-6 && f_time<=174.93e-6) || (f_time>=183.26e-6 &&
f_time<=191.59e-6)
            || (f_time>=199.92e-6 && f_time<=208.25e-6) || (f_time>=216.58e-6 &&
f_time<=224.91e-6)
            || (f_time>=233.24e-6 && f_time<=241.57e-6) || (f_time>=249.9e-6 &&
f_time<=258.23e-6)
            || (f_time>=266.56e-6 && f_time<=274.89e-6) || (f_time>=283.22e-6 &&
f_time<=291.55e-6)
            || (f_time>=299.88e-6 && f_time<=308.21e-6) || (f_time>=316.54e-6 &&
f_time<=324.87e-6)
            || (f_time>=333.2e-6 && f_time<=341.53e-6) || (f_time>=349.86e-6 &&
f_time<=358.19e-6)
            || (f_time>=366.52e-6 && f_time<=374.85e-6) || (f_time>=383.18e-6 &&
f_time<=391.51e-6)
            || (f_time>=399.84e-6 && f_time<=408.17e-6) || (f_time>=416.5e-6 &&
f_time<=424.83e-6)
            || (f_time>=433.16e-6 && f_time<=441.49e-6) || (f_time>=449.82e-6 &&
f_time<=458.15e-6)
            || (f_time>=466.48e-6 && f_time<=474.81e-6) || (f_time>=483.14e-6 &&
f_time<=491.47e-6)
```

```

        || (f_time>=499.8e-6 && f_time<=508.13e-6) || (f_time>=516.46e-6 &&
f_time<=524.79e-6)
        || (f_time>=533.12e-6 && f_time<=541.45e-6) || (f_time>=549.78e-6 &&
f_time<=558.11e-6)
        || (f_time>=566.44e-6 && f_time<=574.77e-6) || (f_time>=583.1e-6 &&
f_time<=591.43e-6)
        || (f_time>=599.76e-6 && f_time<=608.09e-6) || (f_time>=616.42e-6 &&
f_time<=624.75e-6)
        || (f_time>=633.08e-6 && f_time<=641.41e-6) || (f_time>=649.74e-6 &&
f_time<=658.07e-6)
        || (f_time>=666.4e-6 && f_time<=674.73e-6) || (f_time>=683.06e-6 &&
f_time<=691.39e-6)
        || (f_time>=699.72e-6 && f_time<=708.05e-6) || (f_time>=716.38e-6 &&
f_time<=724.71e-6)
        || (f_time>=733.04e-6 && f_time<=741.37e-6) || (f_time>=749.7e-6 &&
f_time<=758.03e-6)
        || (f_time>=766.36e-6 && f_time<=774.69e-6) || (f_time>=783.02e-6 &&
f_time<=791.35e-6)
        || (f_time>=799.68e-6 && f_time<=808.01e-6) || (f_time>=816.34e-6 &&
f_time<=824.67e-6)
        || (f_time>=833e-6 && f_time<=841.33e-6) || (f_time>=849.66e-6 &&
f_time<=857.99e-6)
        || (f_time>=866.32e-6 && f_time<=874.65e-6) || (f_time>=882.98e-6 &&
f_time<=891.31e-6)
        || (f_time>=899.64e-6 && f_time<=907.97e-6) || (f_time>=916.3e-6 &&
f_time<=924.63e-6)
        || (f_time>=932.96e-6 && f_time<=941.29e-6) || (f_time>=949.62e-6 &&
f_time<=957.95e-6)
        || (f_time>=966.28e-6 && f_time<=974.61e-6) || (f_time>=982.94e-6 &&
f_time<=991.27e-6)
        || (f_time>=999.6e-6 && f_time<=1007.93e-6))
        {F_PROFILE(f, th, nv) = 13.89*sin(PI*f_time/8.33e-6);
        }
        else
        F_PROFILE(f, th, nv) = 0;
    }
end_f_loop (f, th)
}

```

## References

1. I.M. Htchings, G.D. Martin, Inkjet Technology For Digital Fabrication, AJohn Wiley & Sons Ltd., Chichester (2013)
2. M.J. McCarthy, N.A. Molloy, Review of stability of liquid jets and the influence of nozzle design, Chem. Engr. Journal, Volume 7, Issue 1, 1974, P1-20
3. J.F. Dijkstra, P.C. Duineveld, Precision ink jet printing of polymer light emitting displays, J. Mater. Chem., 2007, 17, 511-522
4. D. Jang, D. Kim, J. Moon, Influence of Fluid Physical Properties on Ink-Jet Printability, Langmuir, 2009, 25(5), pp 2629-2635
5. X. Zhang, Dynamics of drop formation in viscous flows, Chem. Engr. Science, Volume 54, Issue 12, 1999, pp 1759-1774
6. P. Calvert, Inkjet printing for materials and devices, Chem. Mater., 2001, 13(10), pp 3299-3305
7. P. Shin, J. Sung, Control of droplet formation for low viscosity fluid by double waveforms applied to a piezoelectric inkjet nozzle, Microelectronics Reliability, V 51, Issue 4, 2011, pp 797-804
8. R. Michael, J. Verkouteren, Inkjet Metrology II: Resolved Effects of Ejection Frequency, Fluidic Pressure, and Droplet Number on Reproducible Drop-on-Demand Dispensing, Langmuir, 2011, 27 (15), pp 9644–9653
9. H. Dong, W. Carr, An experimental study of drop-on-demand drop formation, Phys. Fluids 18, 072102(2006)
10. Dong, H.M., Doctoral Thesis. 2006
11. C. Evans, M. Christopher, Optimisation of Ink Jet Droplet Formation Through Polymer Selection, 1999 International Conference on Digital Printing Technologies. pp. 78-81(4)
12. B. Lopez, D. Vadillo, Transient Phenomena During Drop Formation In DOD Printing, 2002 International Conference on Digital Printing Technologies., pp. 170-175(6)
13. D. Xu, V. Sanchez-Romaguera, Inkjet printing of polymer solutions and the role of chain entanglement, J. Mater. Chem., 2007, 17, 4902-4907
14. H. Wijshoff, Structure and fluid dynamics in Piezo Inkjet printheads, Doctoral Thesis, 2008
15. S. Sakai, Dynamics of Piezoelectric inkjet Printing System, 2000 International Conference on Digital Printing Technologies., pp. 15-20(6)
16. J. Dijkstra, Hydrodynamics of small tubular pumps, Journal of Fluid Mechanics, Volume 139, February 1984, pp 173-191
17. J. Cittadino, E. mendes, A Tool for Monitoring Piezoelectric Micro-Pumps, 2005 International Conference on Digital Printing Technologies., pp. 278-282(5)

18. Feng, James Q., A General Fluid Dynamic Analysis of Drop Ejection in Drop-on-Demand Ink Jet Devices, *Journal of Imaging Science and Technology*, Number 5, September/October 2002, pp. 398-408(11)
19. Weast, R. Lide, D. Astle, M. Beyer, W. (1989-1990). *CRC Handbook of Chemistry and Physics*. 70th ed. Boca Raton, Florida: CRC Press, Inc.. F-373,376.
20. Jermy M., "Fluid Mechanics A Course Reader," Mechanical Engineering Dept., University of Canterbury, 2005, pp. d5.10.
21. Hughes, Roger "Civil Engineering Hydraulics," Civil and Environmental Dept., University of Melbourne 1997, pp. 107–152
22. E. M. Purcell. "Life at Low Reynolds Number", *American Journal of Physics* vol 45, pp. 3–11 (1977)[1]
23. Fouz, Infaz "Fluid Mechanics," Mechanical Engineering Dept., University of Oxford, 2001, p. 96
24. McKinley, Gareth H.; Renardy, Michael (2011). "Wolfgang von Ohnesorge". *Physics of Fluids* 23
25. P. Notz, A. Chen, O. Basaran, Satellite drops: Unexpected dynamics and change of scaling during pinch-off, *Phys. Fluids* 13, 549 (2001)
26. F. Tseng, A high-resolution high-frequency monolithic top-shooting microinjector free of satellite drops - part I: concept, design, and model, *Journal of Microelectromechanical Systems*, 2002, (Volume:11, Issue: 5)
27. H. Wijshoff, The dynamics of the piezo inkjet printhead operation, *Physics Reports*, Volume 491, issues 4-5, 2010, pp. 77-177
28. H, Le, Progress and Trends in Ink-jet Printing Technology, *Journal of Imaging Science and Technology*, Number 1, January/February 1998, pp. 49-62(14)
29. Definition of inkjet printer, *pcmag.com*. 1994-12-01
30. G. Wassink, Inkjet printhead performance enhancement by feedforward input design based on two-port modeling, Doctoral thesis, 2007
31. Jet sprayer actuated by supersonic waves, US Patent 2,512,743
32. R.D. Carnahan, S.L. Hou, Ink jet technologies, *IEEE Trans. Ind. Appl.*
33. Pulsed droplet ejecting system, US 3683212
34. Arrangement of writing mechanisms for writing on paper with a colored liquid, US 3747120
35. Method and apparatus for recording with writing fluids and drop projection means therefor, US 3946398
36. Ink jet method and apparatus, US 4459601
37. Shear mode transducer for drop-on-demand liquid ejector, US 4584590
38. R. L. Adams, J. Roy, A One-Dimensional Numerical Model of a Drop-On-Demand Ink Jet, *J. Appl. Mech.* 53(1), 193-197, 1986
39. T. Shield, D. Bogy, A numerical comparison of one-dimensional fluid jet models applied to drop-on-demand printing, *Journal of Computational physics*, Volume 67, Issue 2, 1986, pp. 327-347

40. J. Fromm, Numerical Calculation of the Fluid Dynamics of Drop-on-Demand Jets, IBM Journal of Research and Development, Volume 28, Issue 3, 1984
41. Q. Xu, O. Basaran, Computational analysis of drop-on-demand drop formation, Phys. Fluids 19, 102111 (2007)
42. J. Castrejón-Pita, N. Morrison, Experiments and Lagrangian simulations on the formation of droplets in drop-on-demand mode, Phys. Rev. E 83, 036306, 2011



## Vita

### Name:

Peiding Wang

### Place of Birth:

Sichuan, China

### Education:

B.S. in Thermal Energy and Power Engineering (09/2008 – 06/2012), Harbin

Engineering University, Harbin , China

### Experience

Research and Teaching Assitant (08/2012 – 08/2014), Institute of Research for

Technology Development (IR4TD), Department of Mechanical Engineering,

University of Kentucky